Earthquake Frequency-Magnitude Distribution and Interface Locking at the Middle America Subduction Zone near Nicoya Peninsula, Costa Rica

A Thesis
Presented to
The Academic Faculty

By

Abhijit Ghosh

In Partial Fulfillment of the Degree
Master of Science in Earth and Atmospheric Sciences

Georgia Institute of Technology

August, 2007

Earthquake Frequency-Magnitude Distribution and Interface Locking at the Middle America Subduction Zone near Nicoya Peninsula, Costa Rica

Approved by:

Dr. Andrew V. Newman, Advisor
School of Earth and Atmospheric Sciences
Georgia Institute of Technology

Dr. Zhigang Peng
School of Earth and Atmospheric Sciences
Georgia Institute of Technology

Dr. Dominic Assimaki
School of Civil and Environmental Engineering
Georgia Institute of Technology

Date Approved: June 15, 2007

ACKNOWLEDGEMENTS

I would like to thank my primary advisor Dr. Andrew V. Newman for providing his excellent guidance and scientific insight throughout the study. I am thankful to Dr. Zhigang Peng and Dr. Dominic Assimaki, members of the Thesis Reading Committee, for their thoughtful advice and suggestions. I am grateful to Dr. Tapas Bhattacharyya for the stimulating discussions and his support. I would also like to thank numerous prior and recent earthquake analysts, including Jaime Convers, Grant T. Farmer, Alice Koerner, and Amanda M. Thomas, for their contributions to complete the earthquake catalog. Help of Jana Stankova-Pursley is thankfully acknowledged. I also thank those who participated in the Costa Rica Seismogenic Zone Experiment (CRSEIZE). National Science Foundation grant OCE-9910609 supported CRSEIZE, and Georgia Tech Research Foundation supported this study.

I would like to express my gratitude to my family members, including my fiancée Deblina Datta, for their continuing support.

TABLE OF CONTENTS

LIST OF FIGURES

SUMMARY

Subduction zone megathrusts produce the majority of the world's largest earthquakes. To understand the processes that control seismicity here, it is important to improve our knowledge on the subduction interface characteristics and its spatial variations. Nicoya Peninsula, Costa Rica, extends the continental landmass ~50 km towards the trench, making it a very suitable place to study interface activity from right on the top of the seismogenic zone of the Middle America Subduction Zone (MASZ). We contribute to and utilize an earthquake catalog of 8765 analyst-picked events to determine the spatial variability in the earthquake frequency-magnitude distribution (FMD) in this region. After initial detection, magnitude determination and location, the events are precisely relocated using a locally derived 3-D seismic compressional and shear wave velocity model (DeShon et al., 2006). After restricting the dataset to events nearest the interface and with low formal error (horizontal location error < 5 km), we retain a subset of 3226 events that best resolves interface activity.

Beneath Nicoya, we determine the spatial variability and mean FMD of the interface, and focus on the relative relationship of small-to-large earthquakes, termed *b*-value. Across the region, the overall *b*-value (1.18 ± 0.04) is higher than the global average (*b*~1), and much larger than the global subduction zone average (b~0.6). Significant variation in *b*-value is observed along the active plate interface. A well resolved zone of lower *b* is observed at and offshore central Nicoya coast, in a previously determined locked patch using deformation observed from Global Positioning System (GPS). Conversely, high *b*-values prevail over the subducted portion of the Fisher ridge, which likely ruptured in the 1990 Gulf of Nicoya M_w 7.0 earthquake.

Observed regions of low *b*-value approximately corresponds to more strongly-locked segments of the subduction interface resulting in higher differential stress, which may be released in the next large interface earthquake in this part of the MASZ. Across the region the *b*-value is found to vary inversely with the degree of interface locking. Thus, it is proposed that if sufficient data exist, spatial *b*-value mapping can be used as a proxy to determine interface locking. This method is especially useful along the subduction megathrust, which is generally offshore making geodetic measurements difficult.

CHAPTER 1

INTRODUCTION

1.1 Overview

Plate boundaries are the most seismologically active areas around the world. Convergent boundaries, especially the subduction zones, are very interesting because of their high rate of seismicity and the complexity generated by the combination of different geological processes. This type of plate boundary is characterized by the subduction of a lithospheric plate beneath another making it one of the most active geologic features on the earth. The majority of the world's largest earthquakes are generated at the plate interface of the subduction zones, also known as subduction megathrusts. From the point of view of earthquake hazard, it is important to understand the processes and their interactions that may control the earthquake activity at the subduction interface. In this study, I examine Middle America Subduction Zone (MASZ) near Nicoya Peninsula, Costa Rica to understand the variability in seismicity pattern and earthquake potential along the subduction megathrust. The trench associated with MASZ is commonly referred to as Middle America Trench (MAT).

In this study, I apply the Gutenberg and Richter (1944) earthquake frequency-magnitude distribution (FMD) to study the earthquake activity along the megathrust of this subduction zone. Throughout this study, the main focus is on the parameter *b*, also known as *b*-value, and its variation along the interface. Variation in *b*-value at different tectonic regimes and its interpretation is an active area of research for the past several decades. However a conclusive answer remains elusive. This study

aims to enhance our understanding of the physical meaning of the variation in *b*, as well as its implications in the subduction environment.

1.2 Location

MASZ is situated at the southern-most part of the North America continent. This northwest-southeast trending convergent boundary goes along the western coast of this area. Geographically, the northwestern tip of MAT starts from the middle of Mexico, while it terminates at its southeastern tip in the northern Panama (Figure 1). The total length of the trench is approximately 3000 km. This study examines approximately a 150 km long segment in the southern part of MAT offshore Nicoya Peninsula, Costa Rica. This region is characterized by some of the most complex tectonic features along the MAT (see section 1.3 for details). Here, a part of the subduction thrust plane is investigated with earthquake FMD analysis. Considering the geographic location of the seismic network and the coverage of the local velocity model, a rectangular area is selected which is bounded by the following coordinates (longitude and latitude) at its four corners (Figure 2):

86.37 W, 10.00 N

85.60 W, 10.90 N

84.60 W, 10.05 N

85.37 W, 09.15 N

In the following chapters, the results of the FMD analysis only within this area will be shown and discussed unless otherwise indicated.

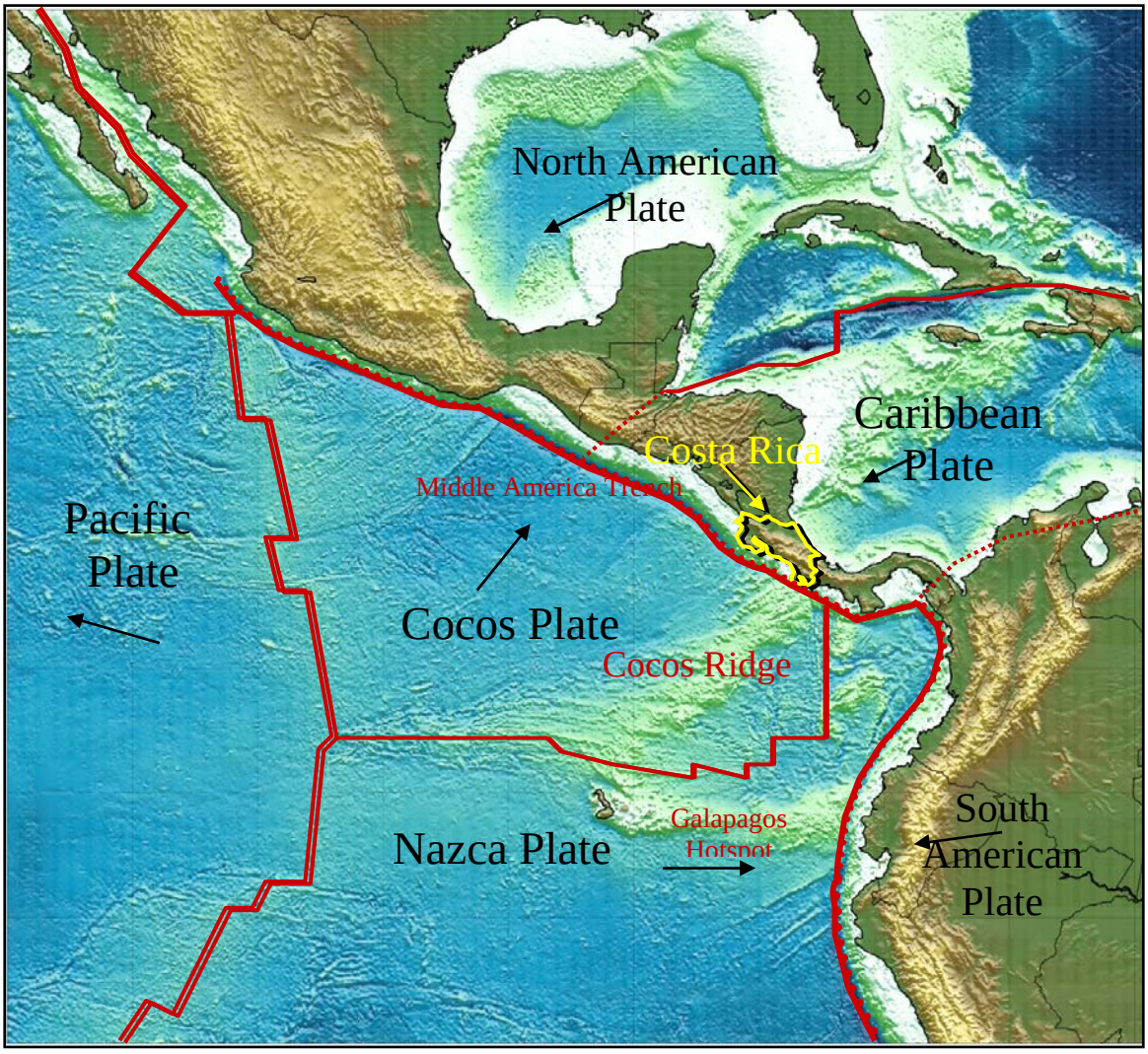

Figure 1: The oceanic Cocos plate subducting beneath the Caribbean plate along the MAT at a rate of ~85 mm/yr (DeMets, 2001) near Nicoya. Notice the rough bathymetry near Cocos Ridge off Nicoya Peninsula, Costa Rica.

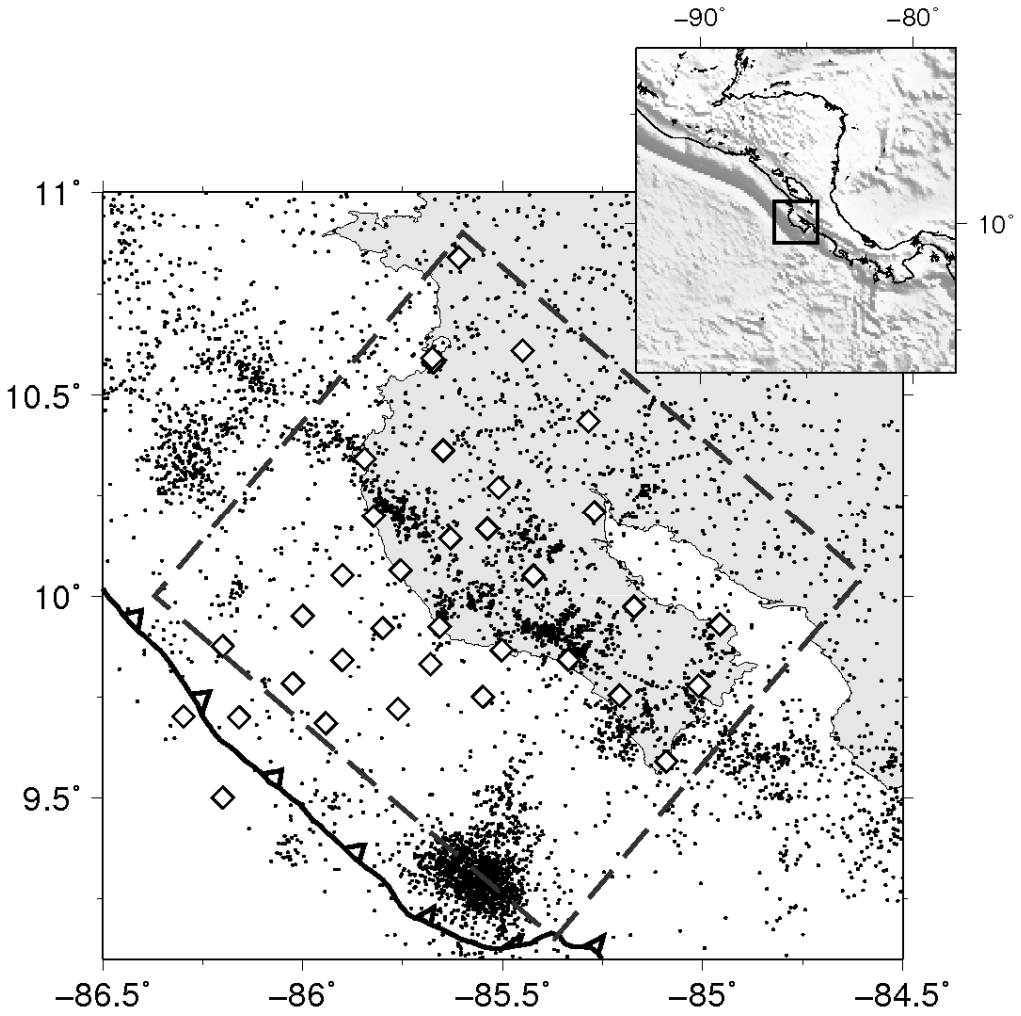

Figure 2: Map of the Nicoya Peninsula, Costa Rica with low error (within 5 km horizontal error) earthquakes (solid squares) recorded between late-1999 to early-2001 as a part of the CRSEIZE project. Open diamonds indicates the location of the seismic stations. Saw-toothed curve represents the Middle America Trench. Dashed box is boundary of grid used for subsequent *b*-value results. [Inset] map of the region with present study area in smaller black box.

1. 3 Tectonic setting

The section of MASZ off Nicoya Peninsula has a very interesting and a complicated tectonic setting. It is a convergent margin characterized by the subduction of the oceanic Cocos plate beneath the Caribbean plate (Figure 1), at 85 mm/year (DeMets, 2001) near Nicoya. This part of the Cocos plate consists of several tectonic and morphological boundaries. The most evident one is the boundary separating two distinct morphological domains, which was identified as early as 1960s (Fisher, 1961). The northwestern part of the Cocos plate has a smooth topography, distinguishing itself from the southeastern part that has a relatively rough bathymetry dominated by numerous seamounts. The rough-smooth boundary is located off the southern part of the Nicoya Peninsula, such that Cocos plate with mostly smooth seafloor is subducting beneath Nicoya. In addition, Cocos plate is composed of materials of two origins and ages. The northwestern part of the plate is originated at the fast-spreading East Pacific Rise (EPR) while the medium-spreading Cocos-Nazca Spreading (CNS) center created the southeastern part of the Cocos plate (Barckhausen et al., 2001). The boundary between these two parts are also subducting off Nicoya, adding to its complexity. Seafloor heat flow measurements and hydrothermal modeling also detect this boundary as an abrupt thermal transition in this part of the Cocos plate (Fisher et al., 2003). Heat flow measurements on the CNS created seafloor are 105-115 mW/m^2, consistent with the conductive models. In contrast, the northern region with EPR generated crust is anomalously cool, with heat flow values of 20-40 mW/m^2. Newman et al. (2002) showed that the seismogenic updip limit changes from 15 km in the south (CNS generated crust) to 20 km in the northern section which is originated at EPR, consistent with the heat flow measurement. At the trench, the crust generated by the EPR is ~24 Ma old (Figure 3), but CNS created crust is almost ~1.5 Ma younger with an age of ~22.5 Ma

(Barckhausen et al., 2001). However, demarcating these different boundaries are challenging considering the fact that this area bears signatures of superimposition of different tectonic, morphological and possibly volcanic activities. Barckhausen et al. (2001) noted at least two tectonic boundaries in this area: the traditional bathymetric rough-smooth boundary associated with a tectonic scarp and the trace of the triple junction between Pacific, Cocos and Nazca plates. Moreover, from the magnetic anomaly map, the authors found a ~80 km long fracture zone trace separating EPR and CNS generated crust. The fracture zone is almost orthogonal to the MAT off the central Nicoya Peninsula. High resolution bathymetric data also show the fracture trace. In the shallow subduction environment across Nicoya, the plate interface changes dip from ~6° near the trench, to ~35° by 40 km depth (Christeson et al., 1999; Sallarès et al., 1999, 2001), before increasing to ~80° down-dip of the seismogenic zone (e.g. Protti et al., 1995a).

The first consistent models for the evolution of the CNS along with the formation of Cocos ridge (further southeast) are given by Hey (1977) and Lonsdale and Klitgord (1978). They proposed that the Farallon Plate broke into the Cocos and Nazca Plates along a preexisting fracture at ~27 Ma. Later, Wilson and Hey (1995) and Barckhausen et al. (2001) revised this model to include a pattern of propagators and two ridge jumps at 19.5 Ma and 14.5 Ma, based on the new magnetic data. The propagator corresponds to a prominent topographic feature, the Fisher Ridge, in the Cocos plate off southeastern boundary of the peninsula. Husen et al. (2002) obtained a tomographic image of what appears to be a subducted seamount associated with the subducting Fisher Ridge. Below the southeastern part of the Nicoya Peninsula, they found a velocity anomaly at a depth of 30 km, and interpreted the zones of higher and lower *P*-wave velocities as the summit and the root of the subducted seamount. This seamount is thought to be the cause of 1990 Mw 7.0 Gulf of Nicoya earthquake.

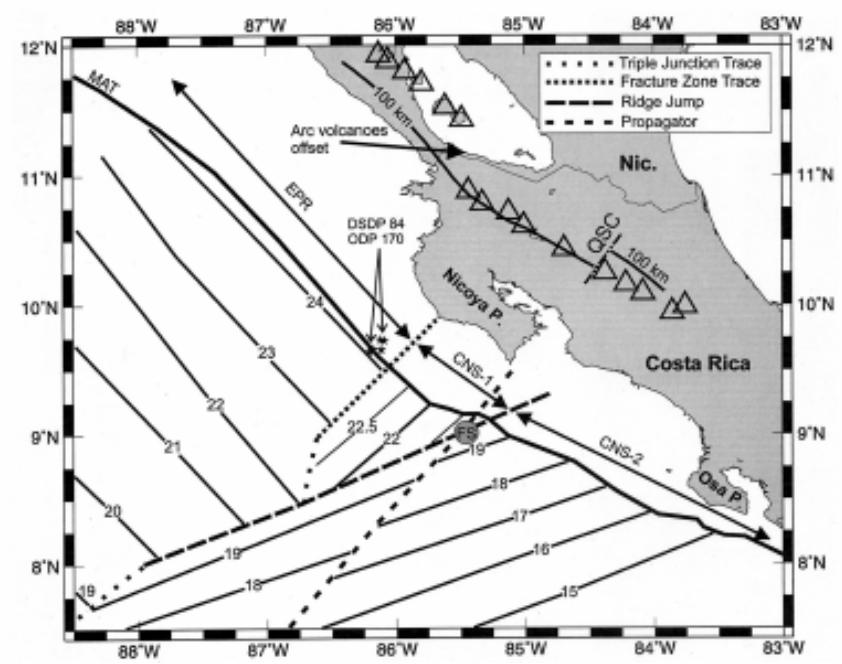

Figure 3: Tectonic map of the study area and its surrounding region. Lines with numbers represent isochrones with ages derived from magnetic anomalies. Triangles are volcanoes. FS, Fisher Seamount; QSC, Quesada Sharp Contortion. (*after* Barckhausen et al., 2001).

1. 4 Motivation and objective

Subduction zones have always been an area of great interest for earth scientists, mainly because of their potential to generate large earthquakes. These earthquakes can not only destroy surrounding areas with strong ground shaking, but also can generate tsunami that may have damaging affect even at the places far from its source, such as the Sumatra earthquake and associated tsunami on 26th December 2004 (Lay et al., 2005). The convergent boundary hosts a combination of geological processes that influences the overall subduction characteristics. The thermal state of the subduction zone, age of the lithosphere, rate of convergence and regional stress regime

are some of the important parameters that significantly control the seismicity pattern here. Most of the large earthquakes occur along the interface of the subduction zone megathrust. Shallow seismicity is mostly concentrated in a narrow band of the interface, called the seismogenic zone.

It is useful to study the characteristics of seismogenic zone and the prevailing stress regime to understand earthquake processes. Properties of the seismogenic zone can vary considerably along the strike, as evident from the along strike shift of updip limit of seismogenic zone at Nicoya (Newman et al., 2002). This part of the MAT interface is also considered to represent a seismic gap that would possibly rupture in a near future large earthquake (Nishenko, 1989), thus it is essential to investigate the along strike variability in megathrust characteristics. Stick-slip behavior in the megathrust is believed to be the cause of large earthquake in the seismogenic zone. Large earthquakes occur at the late stage of 'stick', when the rock cannot sustain the high stress accumulated by the plate convergence. In other words, large earthquakes are associated with locked portions of megathrust, which defines the region of high stress buildup along the interface. Modeling of geodetic data is a conventional way to determine the locked patch along a fault plane. But this technique is mainly dependent on land-based Global Positioning System (GPS) instruments that cannot constrain the strain accumulation near trench, typically sitting 100 km offshore. In this study, a method is developed to use microseismicity to infer the stress regime and its variability of along the megathrust. The objective of this study would be to image the subduction interface in terms of its variability in stress regime, and hence locking. If successful, this technique will be able to delineate the locked part of the interface that accumulates significant stress over the seismic cycle.

Previously, microseismicity had been used in terms of its FMD to demarcate the highly stressed region and/or asperities in the San Andreas Fault

(Schorlemmer and Wiemer, 2005; Schorlemmer et al., 2004; Wiemer and Wyss, 1997). The present study extends this technique to the convergent margin which is generally much larger in dimension and more difficult to study. One of the motivations of this study is to test the usefulness of FMD analysis as a proxy for stress in the subduction environment.

1. 5 Earthquake frequency-magnitude distribution

Scientists have been trying to understand earthquake process for centuries (Darwin, 1845). Many different ways are explored to study earthquakes. Earthquake frequency-magnitude relationship is a way to examine seismic activity in an area. The FMD of earthquakes, which was first introduced by Ishimoto and Iida (1939) and Gutenberg and Richter (1944), has a power-law relationship, such that:

$$\log_{10} N = a - b M,$$

where N is the cumulative number of earthquakes greater than or equal to magnitude M, and a and b are constants describing the activity and slope, respectively. Here, we focus on the parameter b, or b-value, which describes the ratio of occurrence of small to large earthquakes. Globally, b-value is ~1 (e.g., Stein and Wysession, 2003), meaning a 10-fold decrease in seismic activity associated with increase in each subsequent unit magnitude (M). In the past decades, earthquake researchers argued back and forth over the variability of b in different regions. Some authors suggested that it does not vary systemetically in different tectonic regime (Bayrak et al., 2002). But Schorlemmer et al. (2005) and numerous other workers showed that b-value varies significantly between individual fault zones (e.g., Wesnousky, 1994, Schorlemmer and Wiemer, 2005), and even within a particular space and time range (e.g., Nuannin et al., 2005). Though the

absolute value of *b*, and even its variability, may heavily depend upon the accuracy of the earthquake catalog, homogenization of the catalog, calculation technique and algorithm used, several attempts had been made to understand the physical meaning of the *b*-value (Mogi, 1962; Scholz, 1968; Warren and Latham, 1970; Wyss, 1973). However a conclusive answer still remains elusive. The first serious attempt to understand the physical significance of *b* was made by Mogi (1962) when he carried out laboratory experiment to suggest that *b* varies with material heterogeneity. Warren and Latham (1973) found a relationship of *b*-value with the thermal state of the rock. Systematic variation of *b*-value also with depth was reported in California (Mori and Abercrombie, 1997). Scholz (1968) is the first to recognize that *b*-value has a clear relationship with the stress in a volume of rock. In his experimental study, he observed that *b* decreases with the increased stress in the rock. Wyss (1973) took this idea beyond the laboratory, and found similar inverse relationship of *b* and stress in the California earthquake dataset. Over time, seismic networks generally become denser with more technologically advanced instruments capable of recording smaller events. Seismic catalogs are becoming more and more accurate with the help of improved location algorithms, velocity models and increased computational power. Taking full advantage of these positive developments, researchers have recently performed many excellent studies on *b*-value that tend to support its relationship with stress. FMD studies have been extensively used in volcanic areas in Washington, Alaska and Italy (Schorlemmer et al., 2003; Wiemer and McNutt, 1997). High *b* is found to be associated with existence of the magma chambers. This result is interpreted to be the result of low effective stress due to increased pore fluid pressure. Weimer and Benoit (1996) also claim that regions with high *b*-values at the subducting slabs are responsible for magma genesis at Alaska and New Zealand convergent margins. Recent studies with different global and regional seismic catalogs show that *b*-value is significantly lower for events

associated with thrust (Figure 4) as compared to normal and intermediate for strike-slip faulting (Schorlemmer et al., 2005). Because faulting type is directly governed by the orientation and magnitude of stress regime of an area, it is evident that stress has considerable effect on *b*. Based on this result, the authors proposed that *b*-value has an inverse relationship with differential stress, which is in turn tied to the confining pressure. Therefore, *b* can act as a stressmeter in the earth crust. Strong support of this concept came from the fact that the asperity, a locked and highly stressed zone along the fault plane, near the Parkfield segment of the San Andreas Fault is marked by a pronounced zone of low *b* (Wiemer and Wyss, 1997). In fact, 99% of the slip and 95% of the aftershocks of the 2004 M_w 6.0 Parkfield event occurred within the rock volume having low *b*-value (Schorlemmer and Wiemer, 2005). An FMD study of the Sumatra subduction zone shows that the area around the epicenter of two giant earthquakes, 2004 M_w 9.0 and 2005 M_w 8.7 events, occurred within the zones of low *b*-values (Nuannin et al., 2005).

All these evidences strongly indicate that stress is the single-most important factor affecting *b*. Although other features like, material heterogeneity, thermal state may locally influence *b*, they do not seem to have any significant effect on *b* at large scale (Wiemer and Benoit, 1996). Therefore, it is reasonable to use *b*-value to infer the stress regime in a volume of rock provided it is calculated from a rich and robust earthquake catalog.

1. 6 Previous works

As a natural laboratory for earth scientists, the MASZ has been the place of concentrated study for the last several decades. This is, in part, because this region has

a very active interface and complex tectonic history within a relatively small geographic location. One of the important aspects of these studies is to determine the variability of locking along the subduction megathrust. The megathrust beneath Nicoya Peninsula is of particular interest because it represents a seismic gap (Nishenko, 1989). Several attempts had been made to illuminate the state of locking in along this region, using GPS data and modeling.

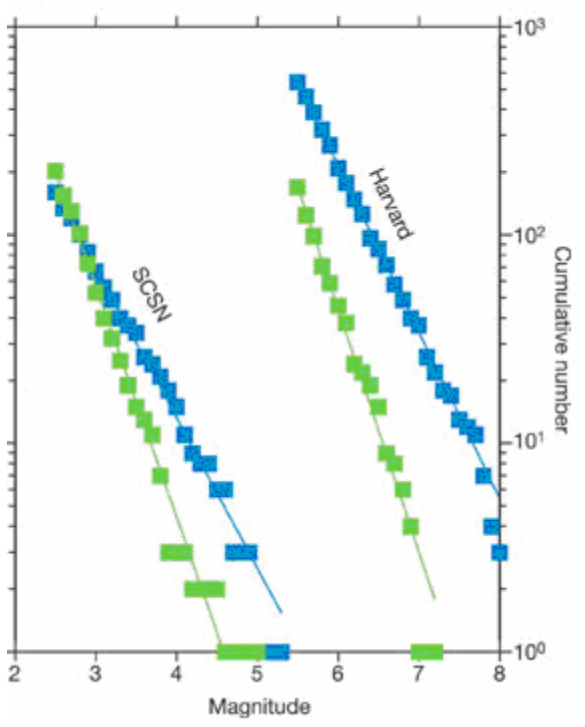

Figure 4: Frequency−magnitude distributions for pure normal (green) and pure thrust (blue) events of the SCSN and Harvard catalogues (Schorlemmer et al., 2005).

Lundgren et al. (1999) first came up with a geodetic model of subduction locking at Nicoya Peninsula. GPS data was collected from 1994 to 1997 in three campaigns. The geodetic network consisted of 14 stations covering the entire peninsula.

The simple dislocation model (Okada, 1985) suggests the presence of a small locked segment from 70 to 95 km downdip from trench. Two different inverse methods are applied to model the coupling between plates. Both the model put forward a heterogeneous seismic coupling along the interface. Central and southeastern Nicoya coast is modeled as strongly locked patches with more than 80% locking. A northwest forearc sliver transport is also detected in this study.

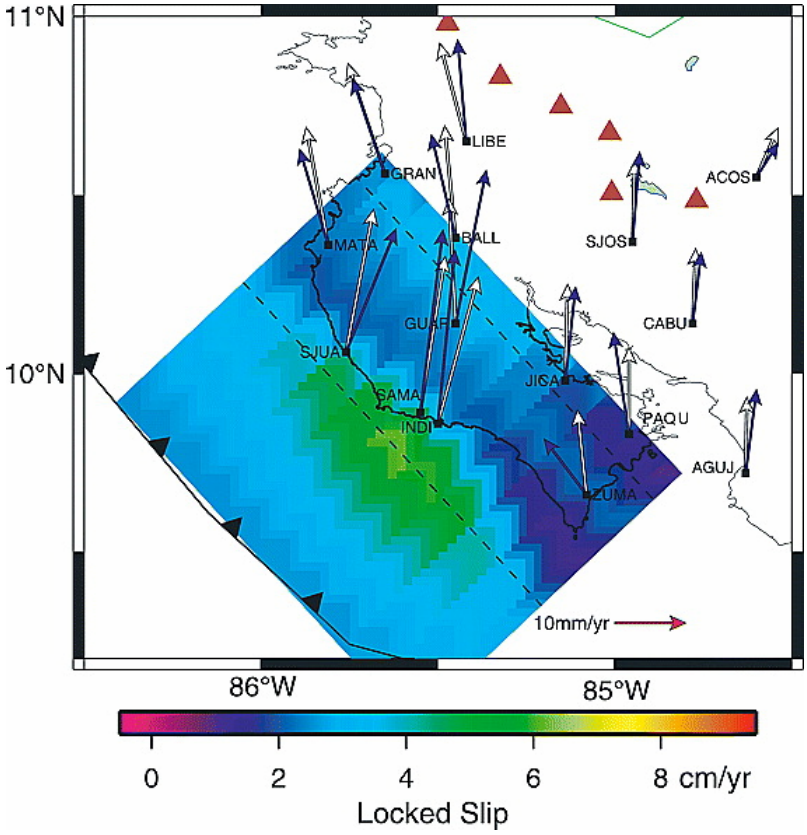

Figure 5: The best fit model for locking along the subduction interface near Nicoya Peninsula using GPS data between 1994 and 2000 (Norabuena et al., 2004). Locking had been modeled as locked slip. Note the elliptical highly locked patch just offshore Nicoya. The near trench updip region which appears weakly locked is poorly constrained due to lack of data in that area.

The network was reoccupied by Norabuena et al. (2004) in 2000. All the data from 1994 onwards are reanalyzed. Their model is better than previous one as this model takes into account both short-term elastic deformation processes and long-term irrecoverable processes that have potential to permanently deform the upper plate. The new model also demonstrates heterogeneous backslip (Figure 5). The most strongly locked patch is centered at 14 ± 2 km depth with a lower one centered at 39 ± 6 km depth. It either indicates a gradational variation of locking at the interface or two distinct locked patches separated by freely slipping zone. However the GPS data could not determine which is occurring in this area. In addition, as in the earlier model, it also found a northwest translation of the forearc block at an average rate of 8 ± 3 mm/yr.

Iinuma et al. (2004) obtained a two-dimensional geodetic model of the area. They analyzed the GPS data from a transect of 10 GPS receivers that extends from the central Nicoya coast to inland Costa Rica, making an approximate straight line perpendicular to the trench across central Nicoya. Data from 3 campaigns within one and half year (from late 2001 to early 2003) are used to calculate velocity vectors. It shows the northwest forearc sliver motion at a rate of ~8.5 mm/yr. To estimate the inter-plate coupling, an inversion analysis with this data had been carried out. It gives the model strain along the line as well as the backslip distribution. The model shows the maximum backslip (and hence locking) just offshore central Nicoya, while it diminishes fairly quickly towards the inland part of the peninsula. Based on the backslip, the authors estimated a future earthquake of M_w 7.5 in this area.

It is worth noting that all the models used slightly different subduction interface geometries. The models are also associated with some inherent simplification and assumptions that may impart significant uncertainty in the model results. Norabuena et al. (2004) did note the sensitivity of their model to the geometry of the interface and the location of the locked patch.

An attempt to determine spatial variation of *b*-value in the Nicoya Peninsula was not successful due to insufficient events in MIDAS catalog (maintained by Middle America Seismograph Consortium) for this region (Monterroso and Kulhánek, 2003). However, an overall *b*-value of 0.92 ± 0.1, calculated using maximum likelihood method with 96 events, is reported for this area.

CHAPTER 2

DATA AND METHODOLOGY

2.1 Seismic Data Acquisition and Processing

Although much work had been done to understand the subduction process along the MASZ, not much high quality seismic data in Costa Rica were available until 1999. The national earthquake catalogs maintained by Observatorio Vulcanológico y Sismológico-Universidad Nacional de Costa Rica (OVSICORI-UNA) and the Red Sismológico Nacional (RSN-ICE) have relatively large error (DeShon et al., 2006) due to limited spatial coverage. A high precision earthquake catalog is the primary requirement to study the seismicity pattern of a region. One of the largest difficulties in accurately constraining the seismogenic extent of the subduction zone is that most subduction megathrusts occur almost entirely offshore, thus making it difficult for land-based techniques to constrain their earthquake activity. However, because the Nicoya Peninsula of Costa Rica extends the shoreline significantly closer to the trench, this region is unique to examine interface seismicity along the megathrust using primarily land-based techniques. To take advantage of this geometry, the Costa Rica Seismogenic Zone Experiment (CRSEIZE) was performed jointly by University of California, Santa Cruz, University of California, San Diego, University of Miami and OVSICORI. The experiment was able to capture much of the ongoing earthquake activity and deformation due to seismogenic zone processes (Newman et al., 2002; DeShon and Schwartz, 2004; Norabuena et al., 2004; DeShon et al., 2006). The seismic component of this project consists of deployment of seismic arrays from mid-September

1999 to June 2001. This total time period had been divided between Osa and Nicoya seismic arrays. However, in this study, I only explore data from the Nicoya seismic array. The Nicoya passive seismic network started working from mid-December 1999 and continues till June 2001. It consisted of 10 short-period and 10 broad-band three component land stations. For the first six months, the network was augmented by a 14 station offshore ocean-bottom (OBS) deployment. Land data acquisition is made in continuous 40 Hz mode, while OBS data were recorded in 64 Hz mode. Land data were quality checked and time corrected using the PASSCAL software (http://www.passcal.nmt.edu/), version 1.9.20 (DeShon, 2004). The seismic array was placed such that it transect the seismogenic zone, and therefore, it was deployed starting from the Cocos plate, very near to the trench, to inland Costa Rica covering the whole Nicoya Peninsula with nearly evenly-spaced land seismic stations (Figure 2). The geodetic component of the CRSEIZE composed of GPS campaigns across Costa Rica that result in a locking map of the interface in this part of MASZ (Norabuena et al., 2004), as discussed in detail in section 1.6.

The seismic array of Nicoya peninsula recorded more than 10,000 local, regional and teleseismic earthquakes. All waveform data were compiled and initial earthquakes locations were determined using the Antelope Relational Database System (version 4.7), developed by Boulder Real Time Technologies Inc. (http://www.brtt.com/). This software gives users the capability to manage and view a large seismic dataset in a graphical user interface (Figure 6). It integrates various algorithms useful for seismological study. In addition, it allows the user to automatically detect earthquakes, filter the waveforms, manually pick different phase arrivals, locate earthquakes, estimate magnitudes and many other analysis techniques that are useful for earthquake studies. However, the automatic detection algorithm within Antelope was not used in this study because the algorithm missed many valuable local events which were important for this

work. Instead, many earthquake analysts, including myself, manually checked the raw waveforms to detect earthquakes and pick first *P*- and *S*-arrivals. Though it has been a very time consuming process, the end product is a high quality earthquake catalog that can be used in this and future seismological studies to understand the seismic process in this area. However, we could not finish picking the events for 58 days starting from the day after the July 21, 2000, M_w 6.4 events. These days are characterized by numerous aftershocks of this large outer rise earthquake. Moreover, including these clustered aftershocks in the FMD calculation may bias the result. So, I decided to exclude these 58 days from the present catalog. The Antelope location algorithm is used for preliminary location of the events from manually picked phase arrivals with IASP91 global velocity model. In total, more than 10,000 events are detected and located using Antelope. The location and phase information are stored in ASCII format that can be easily manipulated for farther analysis.

2. 2 Earthquake Relocation and Magnitude Estimate

The resulting earthquake catalog created within Antelope contains the phase information of first arrivals of *P*- and *S*-wave and locations given by the built-in location algorithm, using IASP91 velocity model. Because the model does not account for lateral seismic wave velocity variations in the earth, initial locations are poorly constrained. Since a spatial FMD study is very sensitive to the event locations, it was necessary to relocate the events using an available 3-D velocity model for this area (DeShon et al., 2006). The velocity model was developed by simultaneous inversion of *P*- and *S*-wave arrival time data of small magnitude local events from this very catalog using the FORTRAN program SIMULPS13Q (Thurber, 1983; Evans et al., 1994). I used

the latest available version of the same program, named Simul2000, to accurately relocate 8765 earthquakes in this catalog. Some events were not relocated due to inadequate phase picks. This improved catalog contains accurate location information with error estimates in all three directions and local magnitude (M_L) estimates. The average resultant horizontal error is 14.52 km, though more than 88% of events contain error within 5 km. Though it does not contain all the events from Julian day 203-2000 to 260-2000 (as mentioned in previous section), It contain approximately 7000 more events than the last study (DeShon et al., 2006) that had been done using this catalog. This high precision rich catalog is a great resource for seismological study in this area.

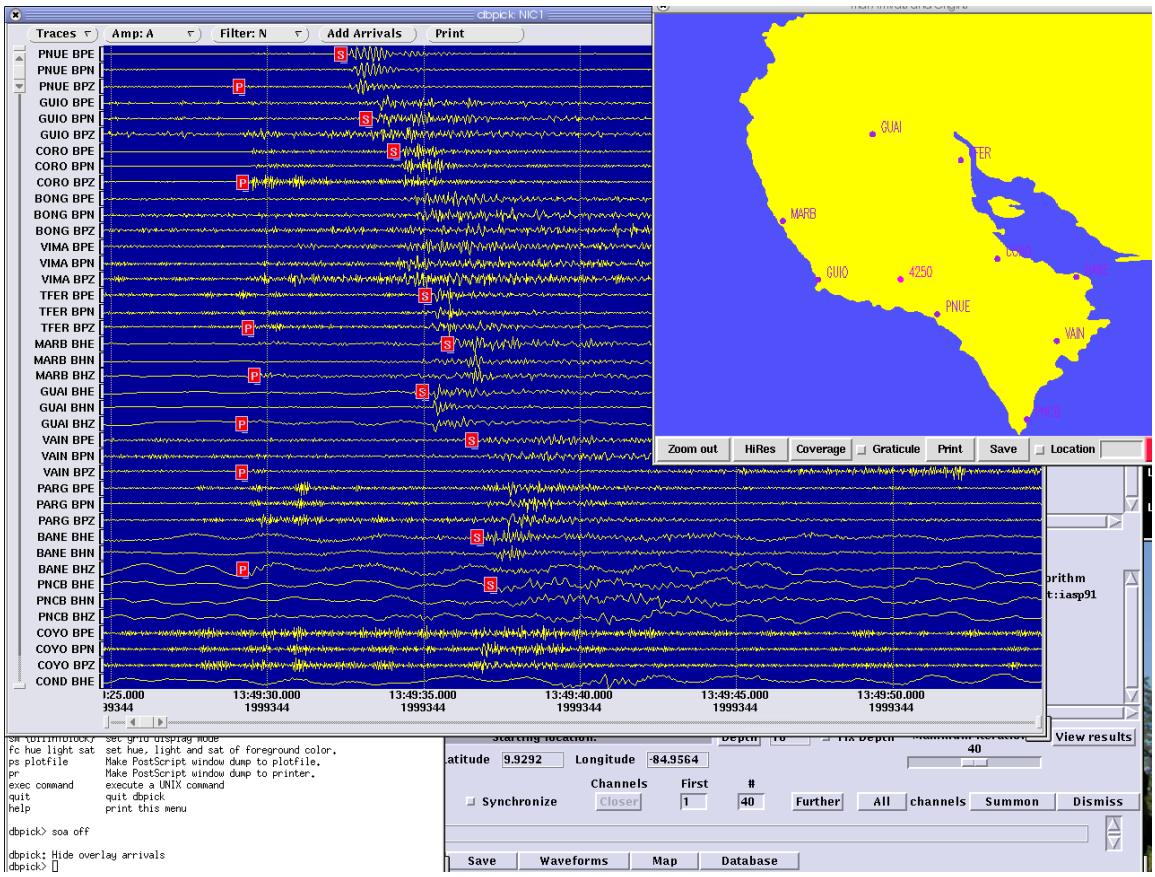

Figure 6: A screenshot of the Antelope program. 'dbpick' window is showing waveform and manually picked first *P*- and *S*-wave arrivals.

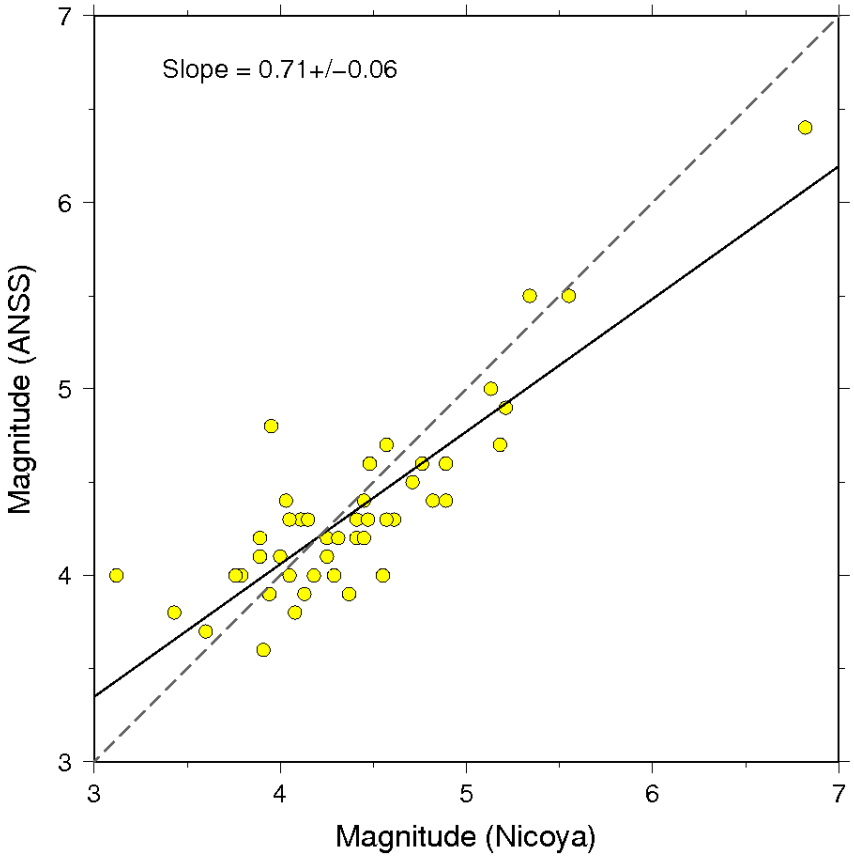

Figure 7: Magnitude comparison between ANSS catalog and Nicoya2000 catalog. Solid straight line is the best fit line (slope = 0.71) between magnitudes reported in two catalogs. Dashed grey line represents the slope = 1.

Along with locations, magnitude estimates are the main parameters of this study. Local magnitudes (M_L) are estimated using the algorithm in the Antelope. Considering the importance of this parameter in this work, I checked the reliability of the magnitude estimates against the Advanced National Seismic System (ANSS) global catalog (http://www.ncedc.org/anss/). This composite global catalog is created by merging different catalog from allover the world and removing duplicate solution for the same event. It is a result of the effort of Council of National Seismic System (CNSS),

USA. I selected the events that are recorded in both the ANSS and the catalog I used here, and compare the magnitudes of these events (Figure 7). The comparison shows a reasonable fit with a slope of 0.71 ± 0.06. More than 90% of the event magnitudes fall within the range of ± 0.5. It is important to note that ANSS catalog does not only report M_L, but it gives different types of magnitude estimates for different events, because it is a combination of various earthquake catalogs. For this comparison, all types of magnitudes reported in the ANSS catalog is taken into account. Considering this fact, magnitude estimates of Nicoya catalog seems reasonably good.

Throughout this study, this catalog, with high precision location, timing and magnitude (M_L) estimates, henceforth called Nicoya2000 earthquake catalog, is used for this spatial FMD study.

2. 3 Calculation of Frequency-Magnitude Distribution

Now that a robust earthquake catalog exists for Nicoya Peninsula, the next important step is to develop an algorithm and associated codes to accurately calculate *b*-values and its spatial variation in this region. Though the Nicoya2000 earthquake catalog contains 8765 earthquakes, I exclude 58 days of earthquakes, as mentioned in the preceding sections, and used only 6620 events with low formal location error ($\sigma_{horiz} \leq$ 5 km) to assure a higher quality result. *b*-value mapping was done at several major faults (Wiemer and Benoit, 1996; Monterroso and Kulhánek, 2003; Schorlemmer and Wiemer, 2005; Nuannin et al., 2005). Most of these studies including those of the subduction zones used all the available earthquakes in the catalog within an area to map spatial variation of *b*, irrespective of the orientations of the faults and the nature of seismicity around it (Wiemer and Benoit, 1996; Schorlemmer and Wiemer, 2005; Nuannin et al.,

2005). This method can significantly increase the number of events to evaluate. However, all the earthquakes evaluated may not be associated with the fault under consideration. Including the off-fault events in the *b*-value calculation may produce artifacts in the spatial *b*-value map that no longer represents processes along the fault interface as these events may represent a completely different stress regime as compared to the major fault plane itself. This factor is particularly important in subduction zones, because the seismicity produced here is the mixture of crustal and interface events which may represent vastly dissimilar states of stress. Since the objective of this study is to investigate the seismicity produced at the subduction interface, it is important to eliminate crustal earthquakes and select the events that best represent the interface seismicity. To minimize the effect of crustal and off-interface earthquakes in the *b*-value calculation, I select the events that define the Wadati-Benioff zone for the study area using a spatially varying polygon. Using this subset of seismicity, a best fit parabolic function is derived [$(114.8 - x)^2$ / 130.7; where x is the distance in km perpendicular to the trench] to farther refine the interface activity. This function represents the best approximation of the interface on the basis of seismicity. Finally I retain only events within 10 km of this parabolic function (Figure 8). After employing this procedure, most of the seismicity associated with July 21 M_w 6.4 outer rise mainshock is eliminated, resulting in a homogenized version of the main Nicoya2000 catalog. This refined catalog contains 3226 earthquakes that best represent the interface activity and is used for farther analysis. It is important to note that although considerable effort is made to separate the interface earthquakes, it is practically impossible to distinguish interface events from those generated at other smaller scale faults surrounding it, especially at the crustal region (up to 15-20 km depth from surface). This is because we still do not have a clear seismic image for most part of the subduction interface, and it can be imagined as the complex combinations of smaller faults that can generate earthquakes with

different fault mechanisms. The method describe above may be the only reasonable way to approximately separate the interface activity, from most intra-plate seismicity down to such a small magnitude.

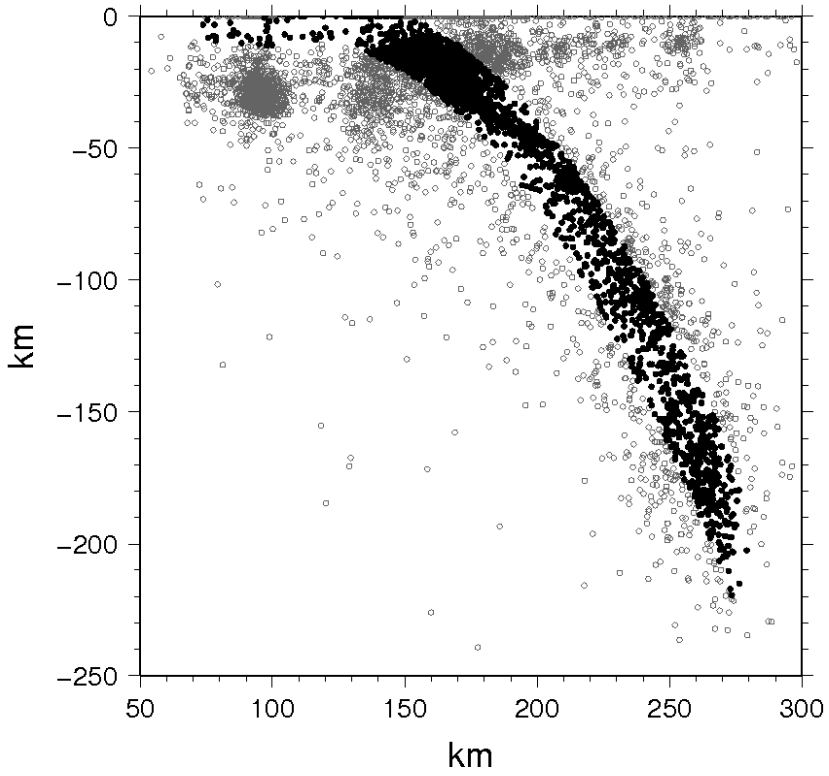

Figure 8: Vertical cross-section of low error CRSEIZE seismicity (open circles). Solid circles represent events defining subduction zone seismicity. Only these events are considered for the frequency-magnitude distribution in this study.

This subset of events is analyzed in terms of its FMD for spatial variability of *b*-value along the interface. Wiemer (2001) developed software called *ZMAP* that is able to compute spatial variation in *b*-value. Instead of using *ZMAP*, similar algorithm and codes are developed that are more suitable for this particular study. My program named *bval*, can generate a spatial map of *b* given a earthquake catalog, like *ZMAP*

does. In addition, users can define a sampling radius which is useful to exclude nodes that have severely smoothed *b*-values. By doing so, the areas which do not have enough events to calculate meaningful results are removed.

The program *bval*, takes an earthquake catalog written in a specific format as the only input file. It automatically makes a grid of the study region. In this work, I created a square grid with uniform 0.02° (approximately 2 km) spacing. After that, it goes to each grid-node and finds the closest 200 events in the catalog in vertical cylindrical volume. Both the grid-spacing and the event number can be modified as needed. From now on, all the computation in that node is done using these selected 200 events. First, it calculates the magnitude of completeness (M_C) and eliminates all the events having magnitudes less than M_C. Then it determines *b*- and *a*-value and associated standard error using both the maximum likelihood (Aki, 1965) and least square fit methods. *bavl* loops over all the nodes to compute these values for each node and stores in an output file. Finally, it brings up a color-coded contour plot of *b*-value only considering the nodes which have the sampling radius less than or equal to that is defined by the user. I use 60 km maximum sampling radius for this study. Determining a useful sampling radius is a trade-off between the spatial extent one would like to have and the smoothing of *b* that can be tolerated. After several tests, 60 km appears to be a good compromise that gives a reasonable spatial extent without loosing too much on the smoothing factor.

The methods used by *bval* for calculating M_C and *b*-value warrant some discussions. For M_C calculation, I used maximum curvature method which had previously been used in several FMD studies (Wiemer and Katsumata, 1999; Wiemer and McNutt, 1997). This method simply picks the point of maximum curvature in the non-cumulative FMD curve. Though it is a widely used technique, it tends to underestimate M_C because in most of the cases, FMD does not have a perfect linear logarithmic fit. Instead, it tends to gradually fall back from the linear trend near estimated M_C and when

it approaches towards large magnitudes. The deviation of FMD near M_C is due to the underestimation of M_C by maximum curvature method. On the other hand, it is an easy and quick method and gives a good first hand estimate of M_C that can be successfully used in spatial FMD study. Wiemer and Wyss (2000) devised a way to compute M_C on the basis of synthetic FMD. But it is rather complex method compared to the maximum curvature. The authors also showed that the average difference in M_C between the two methods is not much (0.13). To account for this difference, a constant shift of M_C (of may be 0.2, to have a more reserve M_C) can be applied, but it may significantly reduce the number of earthquakes available for FMD calculation which adversely affect the quality of the estimates of *b*, as well as its spatial resolution. Hence, it seems that maximum curvature method is the optimum method for a reasonably good estimate of M_C. Throughout this study, I use maximum curvature method to estimate M_C.

For calculation of *b*- and *a*-value, I used both least square fit and maximum likelihood methods. Least square fit is a simple mathematical procedure to compute the best fitting line (or curve) to some data points by minimizing the sum of the squares of the differences between the line and the corresponding points (Scheaffer and McClave, 1986). Standard error in this method is calculated using the following equation:

$$err = \sqrt{\left(\sum (y - \hat{y})^2 / (n - 2) \right)}$$

where, y = actual data, $\hat{y}$ = estimate of y, n = number of data, err = standard error. Here, standard error is used same as standard deviation. It works reasonably well for calculation of FMD parameters. But in most of the cases, FMD deviates significantly near the large magnitude events, particularly in an earthquake catalog which covers only slightly more than 16 months of seismicity. This deviation imparts significant error in *b*-value calculation.

This problem can be avoided by using maximum likelihood method to estimate *b* (Aki, 1965). This method calculates *b* using the following equation:

$$b = \log_{10}(e) / (M_{mean} - M_C)$$

where, M_{mean} = mean magnitude, M_C = magnitude of completeness, e = 2.718281…(base of the natural logarithm). The standard error is given by Shi and Bolt (1982) which is as follows:

$$err = 2.30b^2\sigma(M_{mean})$$

and σ is given by,

$$\sigma^2(M_{mean}) = \sum (M_i - M_{mean})^2 / n(n\text{-}1).$$

The maximum likelihood method is mainly dependent on the smaller magnitude part of the FMD, thus does not has much effect of the deviation at the large magnitude region. It also requires an accurate estimate of M_C. Although both least-square fit and maximum likelihood methods are used in previous *b*-value studies, the latter technique seems to give better estimate of *b* because of its efficiency to avoid the deviation in FMD. It also becomes a generally accepted method in the FMD studies in recent years. Although, *bval* has the ability to compute *b* using both the methods, I primarily use the results given by the maximum likelihood method for interpretation purpose.

CHAPTER 3

RESULTS AND DISCUSSIONS

3.1 Earthquake Relocation

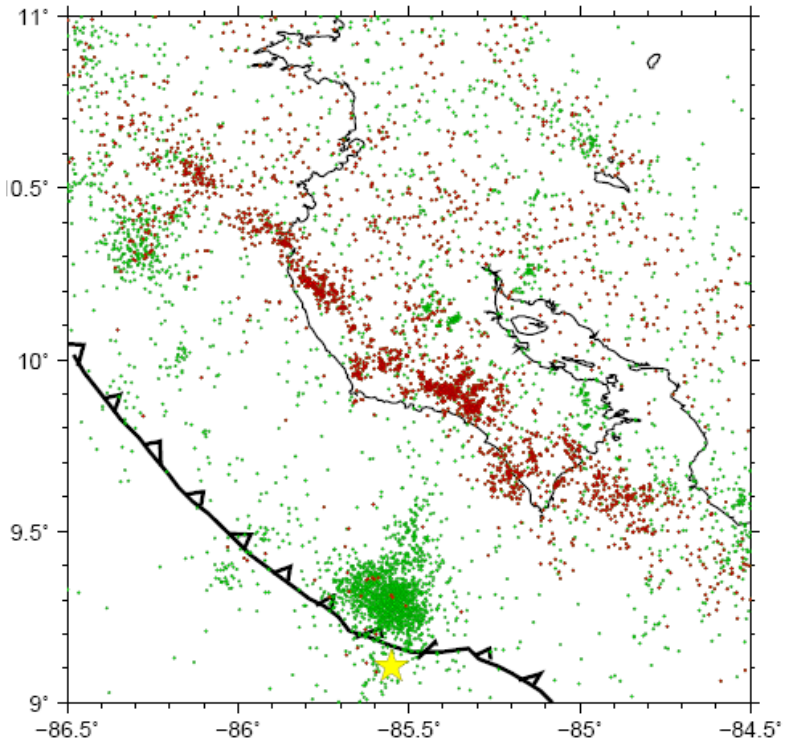

Figure 9: Seismicity in the study area from the present catalog. Saw-toothed curve represent MAT. Red solid circles show interface events with horizontal error within 5 km. Green solid circles show non-interface seismicity. Yellow star represents July 21, 2000 M_w 6.4 event at the outer rise. Note that the aftershock cluster is landward of the trench. Also notice the strong seismic lineation (red events) along the coast of the Nicoya.

The relocated earthquakes show interesting features. The most prominent feature is the clustering of the aftershocks of the July 21, 2000 M_w 6.4 event (Figure 9). The mainshock is a result of the normal faulting located at the shallow part of the outer rise, the seaward side of the MAT. But interestingly, most of the aftershocks are concentrated towards the landward side of the trench, north of the mainshock. They are mainly located beneath the subduction interface and not associated with interface activity (Figure 9). Though the mainshock was denoted as an outer rise event (DeShon et al., 2006; Norabuena et al., 2004) and located seaward of the trench, the spatial distribution of the aftershocks strongly suggests that most slip occurred landward of the trench and lies within the subducting slab. Because the faulting mechanism is normal and the mainshock is located landward of the trench, it is likely that it was caused by the extension of the downgoing Cocos plate.

Perhaps the most intriguing seismic feature in this area is a strong seismic lineation trending northwest-southeast along the coast of the Nicoya Peninsula. It becomes extremely prominent when only interface seismicity is considered (Figure 9, and 10), suggesting the majority of the events occur along a narrow band on the interface. This linear seismic feature is very persistent along the entire Nicoya coast. It implies that the seismic lineation is a result of large scale tectonics in this area rather than smaller scale features like asperity and/or locking on the fault plane. When compared with the subduction interface geometry for this region (Figure 10) derived by Thomas et al. (2007), it reveals some interesting aspects of subduction processes here. The seismic lineation corresponds well with the 20 km depth contour, also trending northwest-southeast, of the subduction interface, and is where the subduction interface changes its dip sharply from a shallow ~10º to a steep ~40º. This abrupt and large change in the dip of the subduction interface can be observed beneath the entire Nicoya coast, similar to the seismic lineation. The sharp change in the dip results in the strong

bending of the interface. This linear zone of strong bending of the subducting slab at 20 km depth may cause frequent rupture along this zone to accommodate the bending producing the linear pattern of seismicity along this region. This finding depicts that subduction interface geometry plays an important role in pattern of earthquake production in and around Nicoya.

A close perusal of interface geometry also shows a sudden along strike bend in the interface depth contours suggesting a contortion of the interface beneath central Nicoya (Figure 10). It indicates that the interface suddenly become shallower at the southeastern side of contortion. A slight shift in the line of seismicity is also observed in this region. This zone of interface contortion corresponds well with landward projection of fracture trace on the Cocos plate (Figure 10). The fracture trace separates the CNS from EPR generated oceanic crust (Barckhausen et al., 2001) while the corresponding interface contortion marks the boundary between the shallower (southeastern side) and deeper (northeastern side) part of the interface. The shallower part at the southeastern side of the contortion (and the fracture trace) is characterized by the subduction of CNS generated oceanic crust which is ~1.5 Ma younger than the EPR created crust at the northwestren side. Moreover, orientation of the seafloor magnetic anomaly suggest that the age difference between CNS and EPR crust across the fracture trace increases as one goes landward form the trench (Figure 3). At the interface contortion, the age difference should goes up to ~3 Ma. Barckhausen et al. (2001) pointed out that the subducted extension of the fracture trace may be a more pronounced feature. In addition, CNS crust produced higher heat flow measurements and modeled as the warmer part of the Cocos plate relative to the EPR crust (Fisher et al., 2003). These evidences suggest that CNS crust is possibly less dense than EPR one. The difference in densities may be the reason of the difference in the depths of the subduction interface across the contortion (and the fracture trace). The CNS crust in the southeastern side is

shallower because of its low density relative to the EPR crust at the northwestern part of the Cocos plate. It appears that the fracture trace is an important tectonic boundary and has significant effect on the interface geometry.

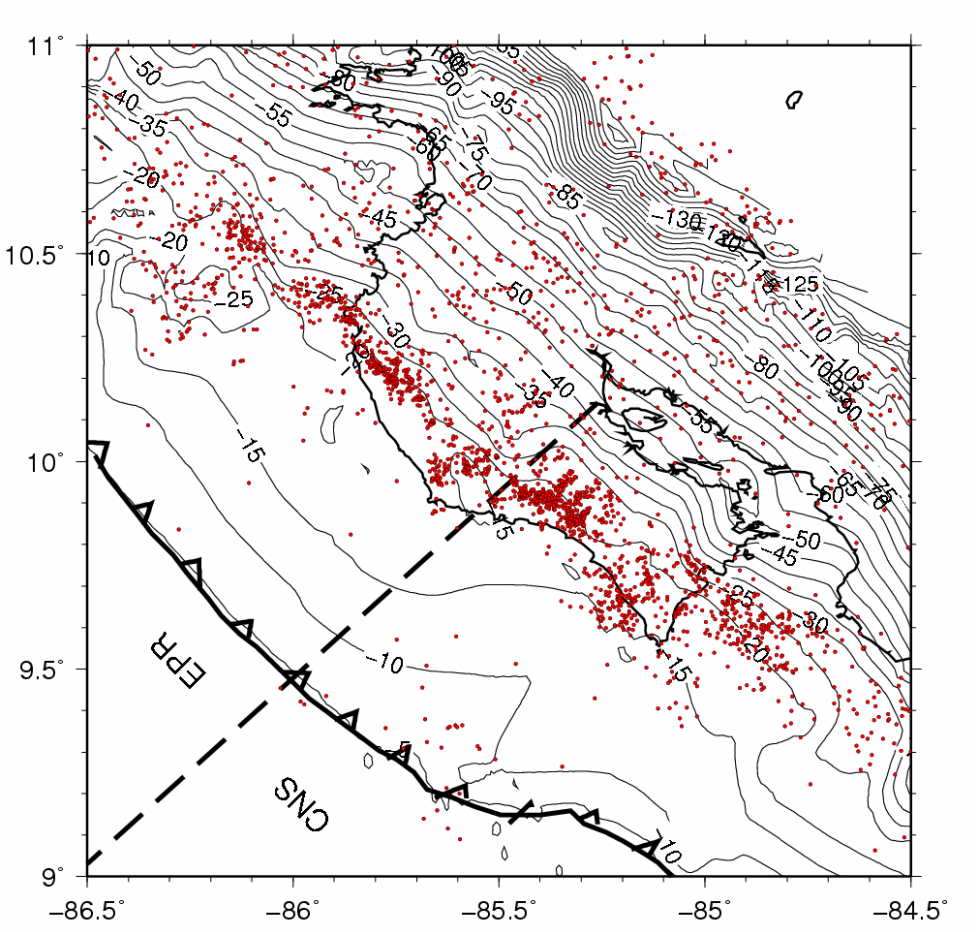

Figure 10: Interface seismicity and subduction interface geometry in the study area. Saw-toothed curve represent MAT. Red solid circles show only interface events with horizontal error within 5 km. Contours in km from mean sea level represent subduction interface geometry for this region derived by Thomas et al., 2007. Note the bend in the depth contours of the subduction interface beneath the central Nicoya. Dashed grey line represents the trace of the fracture zone in the Cocos plate and its landward projection. Notice that dashed line corresponds well with the bending of the depth contours.

3.2 Overall Frequency-Magnitude Distribution

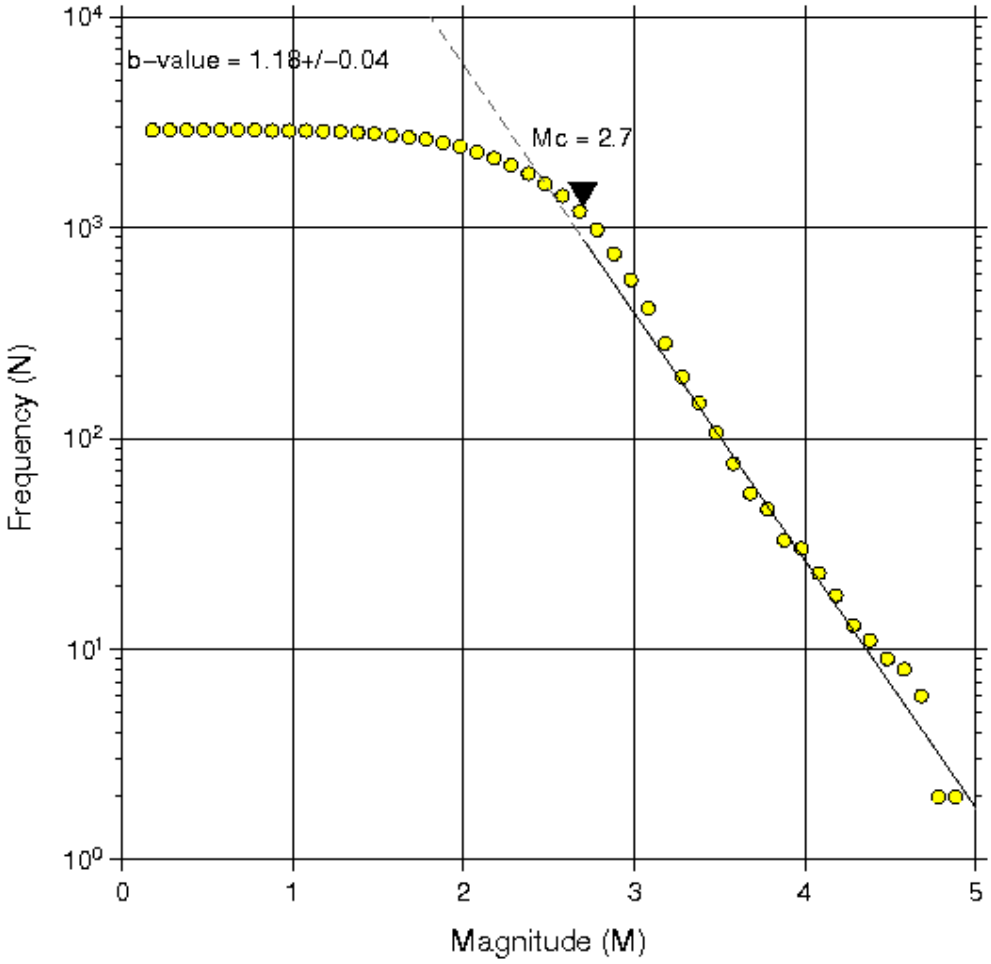

Figure 11: Overall *b*-value of the subduction interface off Nicoya Peninsula calculated using the maximum likelihood method.

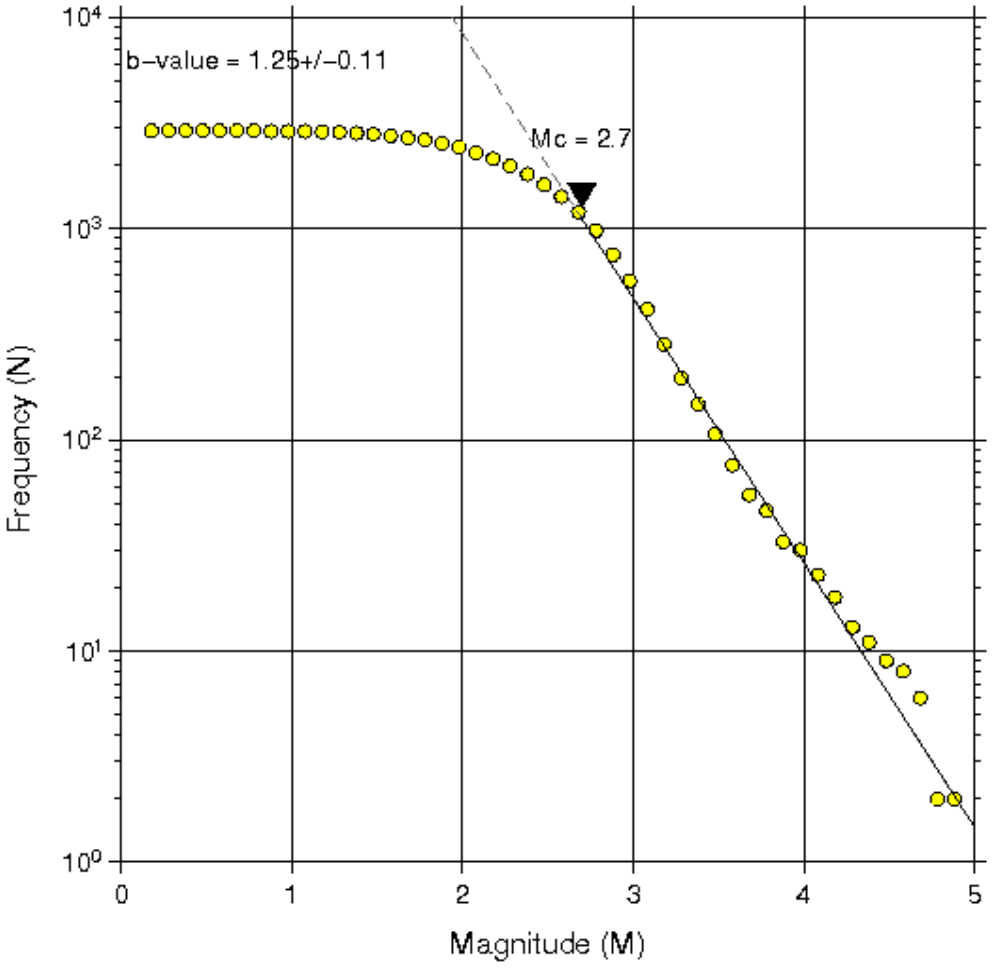

Figure 12: Overall *b*-value of the subduction interface off Nicoya Peninsula calculated using the least square fit method.

Results of this FMD study shows some very interesting features. Before going into the details of spatial FMD mapping, I would like to present the overall FMD for this area. The overall *b*-value estimate for the Nicoya subduction interface using the maximum likelihood method is found to be 1.18 (Figure 11) with a standard error of 0.04 (3%). A least squares estimate gives similar results with a *b*-value of 1.25 (Figure 12) and somewhat larger error of 0.11 (9%). The M_C is calculated to be 2.7 using the

maximum curvature method for the entire interface catalog. Shifting M_C by 0.2 towards a more conservative estimate does not produce much change in *b*, such that the maximum likelihood *b* is estimated to be 1.23 with 0.05 standard error and the least square method gives a value of 1.24 with a standard error of 0.12. The larger error in *b*, when calculated with a more conservative M_C of 2.9 is possibly attributed to the fact that approximately 45% data are lost due to the small (in this case, 0.2) increase in M_C. In addition, using both the methods of M_C calculation, the *b* estimates look very similar. Hence, the cost of a more reserve M_C is too high in this study with not much change in the results; therefore, the maximum curvature method is also used for spatial FMD analysis.

The global average of *b* is observed to be approximately 1 (e.g. Stein and Wysession, 2003), which is a little lower than that is found here. Interestingly, the world-wide subduction zone *b* shows an even lower value with a range of 0.53 to 0.74 (Bayrak et al., 2002) mainly because the seismicity here is dominated by thrust faulting (Schorlemmer et al., 2005). In contrast, Nicoya subduction megathrust has relatively large *b* (1.18). As discussed in the section 1.5, relatively higher *b* indicates lower stress. Thus larger *b* in Nicoya compared to the global average apparently suggests a generally weak interface in this region. But it should be noted that most global FMD studies are based on relatively spatially unfiltered global earthquake catalogs over long time periods. However, in this study I used a local seismic catalog that spans only ~16 months. Moreover the events used in this study represent only subduction interface activity without much contamination from the crustal events. Therefore, comparing the outcome of this work directly to the global FMD study may results in misleading interpretations. For example, Southern Tyrrhenian Subduction Zone in Italy shows an overall *b* of 1.64 based on a regional catalog provided by the Istituto Nazionale di Geofisica e Vulcanologia (Schorlemmer et al., 2003). An overall *b* of 1.14 ± 0.13 is reported from

New Zealand subduction zone using a regional catalog compiled by the Seismological Observatory, Institute of Geological and Nuclear Sciences in New Zealand (Wiemer and Benoit, 1996). This part of the New Zealand subduction zone had been identified as strongly locked (Reyners, 1998), and hence an area of strong seismic coupling. Nuannin et al., (2005) came up with the most striking example when they analyzed FMD of earthquakes reported by United States Geological Survey spanning a time period of five years, preceding the great Sumatra 2004 M_w 9.0 event, in Sumatra and Andaman-Nicobar Island subduction zone. They found an overall *b*-value of 1.21 ± 0.13 for this region. Occurrence of the great earthquake suggests that the subduction megathrust was a region of very high stress accumulation (strong seismic coupling). All the studies mentioned above are done using *ZMAP* which uses the maximum likelihood method to compute *b*, negating any possible effects on the magnitudes of *b* due to difference in calculation methods. In the light of these recent works, it seems that Nicoya subduction interface, with *b*-value of 1.18 ± 0.04, may represents a megathrust with high stress concentration. The main cause of high stress concentration in a large scale tectonic feature like subduction megathrust is the seismic coupling. Comparing the overall *b*-value of Nicoya to the global and regional FMD studies, it appears that the subduction interface near Nicoya Peninsula may be a region of moderate seismic coupling. Geodetic model also shows a combination of locked and freely slipping patches on the interface in this region (Norabuena et al., 2004). Another important factor that may significantly affect the stress accumulation along a fault plane at a particular time window is the stage of seismic cycle under investigation. Irrespective of the nature of seismic coupling (strong, moderate or weak), high stress accumulation likely to occur only at the last stage of seismic cycle. Thus the high stress concentration along the interface near Nicoya possibly indicates that it may be close to the end of a seismic cycle which eventually will terminates in a large earthquake in recent future. This inference is

supported by the long history of devastating “50 year” earthquakes (magnitude ~7.7 or larger) that occurred in this region in 1853, 1900 and 1950 (Brown et al., 2006). However, it is important to note that the overall *b*-value (1.18) for this area should not be taken as a typical value for all subduction megathrust with moderate seismic coupling that is at the last stage of a seismic cycle. It may vary from one subduction zone to another depending upon the seismic network, accuracy of the velocity model and event locations, type of magnitude and methodology used for b-value calculation.

Although overall *b*-value can give a broad idea of the prevailing stress regime in an area, it lacks the spatial detail. In the next section, I will address this issue with the help of the spatial distribution of *b*.

3.3 Spatial Frequency-Magnitude Distribution

The overall *b*-value of Nicoya subduction interface suggests moderate seismic coupling between the overriding and subducting plates. In Nicoya, the coupling, or locking generally varies over the interface (Norabuena et al., 2004) covering several thousand square km, and the next large event is most likely to occur at the zone of the strongest locking and high stress accumulation. The most challenging work in subduction zone earthquake hazard analysis is to delineate this zone. I used spatial FMD mapping to understand the stress regime along the interface, and infer the state of locking. Before calculating *b*, spatial distribution of M_C is determined with the maximum curvature method. In this region, M_C varies from 1.5 to 2.7. The lowest M_C is observed near central Nicoya and offshore and the highest M_C appears near the four corners of the rectangular study area (Figure 13). As M_C is calculated at each grid node, and the

events below M_C's are eliminated before computing *b*, so that the variability in M_C should not affect the *b*-value.

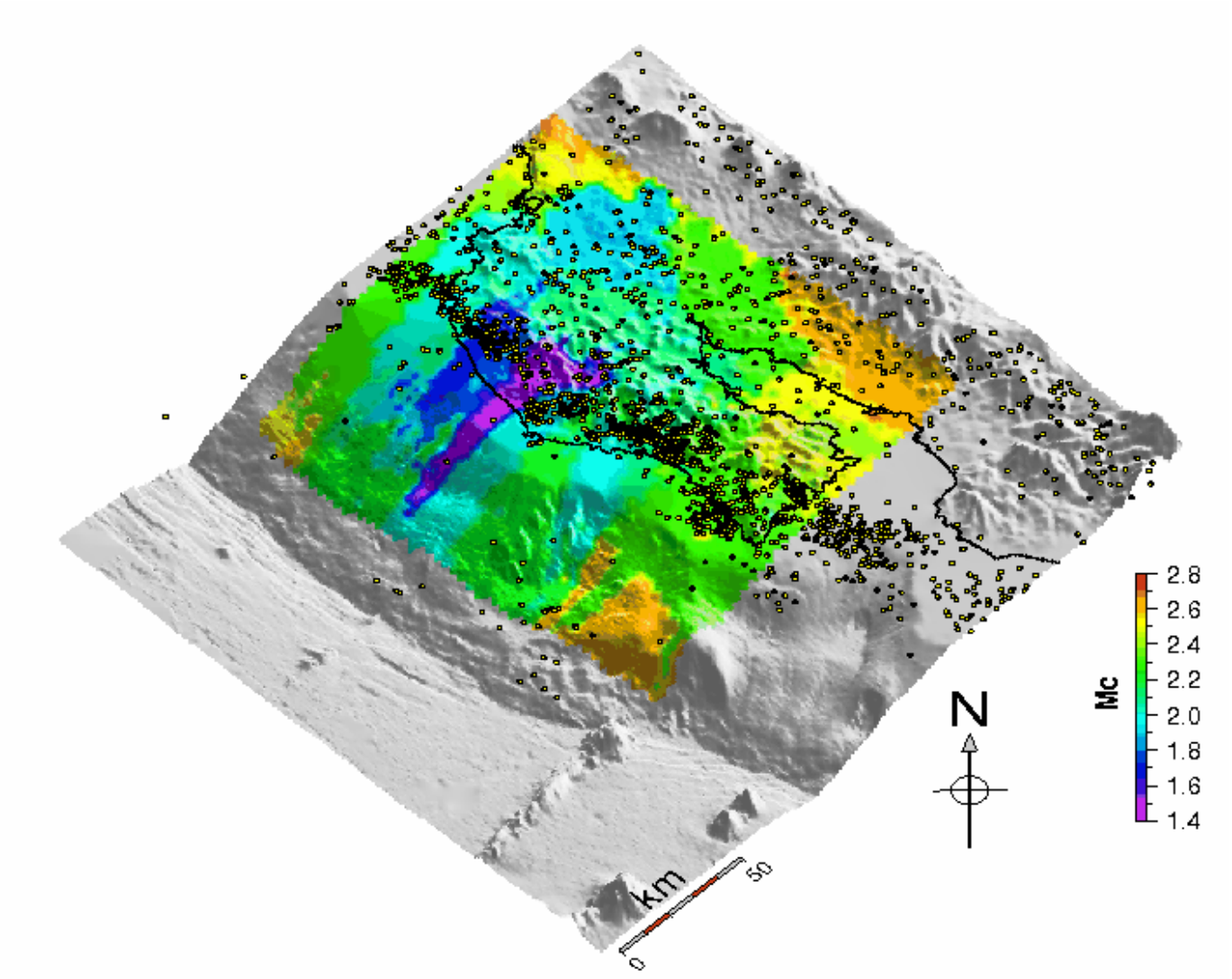

Figure 13: Spatial distribution of M_C calculated by the maximum curvature method. The lowest curvilinear bathymetric feature represents MAT. Yellow solid circles show epicenters of interface earthquakes used for the calculation.

b shows a wide variation along the interface in this region. The maximum likelihood estimates of *b* vary from 0.63 to 1.98 (Figure 14). The standard errors in the estimates range from 4.9% to 20.9% of *b*-value, but for approximately two-third of the data, it is within 10% (Figure 15). The *b*-value distribution, when calculated with the least square fit method, shows similar spatial pattern but with a little higher magnitude of *b* (Figure 16), as also noticed in the overall *b*-value. In this case, *b* varies from 0.73 to 2.79, while the standard error fluctuates from 2.1% to as high as 33.6% (Figure 17). However, approximately 60% of the data contain error within 10%. The spatial pattern of the *a*-value (seismicity rate) looks similar to that of *b*, and it varies between 3.07 and 6.56 (Figure 18). The minimum sampling radius is found to be 5.24 km and the maximum is chosen as 60 km. But at approximately 74% of the total grid nodes, 200 events are found within 40 km radius. The sampling radius is relatively small along the entire peninsula and it gradually increases at the edges (Figure 19). The average resolution, meaning the number of events available after removing the ones below M_C, is approximately 80 per node.

I also tested the spatial variability of *b* with a more reserve estimate of M_C, by increasing M_C by 0.2 from that calculated using maximum curvature method. The distribution of *b* is again very similar to that discussed earlier (Figure 20), though the magnitude of variation is little higher (0.67 to 2.63). Interestingly, the error goes up from the previous method to vary from 6% to 37% (Figure 21), because more than 40% of the data is eliminated as a cost of increasing the M_C by 0.2. The average events per node reduced to approximately 48 from 80 per node in the earlier method. The sharp decrease in the event number can adversely affect the *b*-value estimate, as evident from the enhanced error. Hence, M_C estimated using maximum curvature method is used for this spatial FMD analysis.

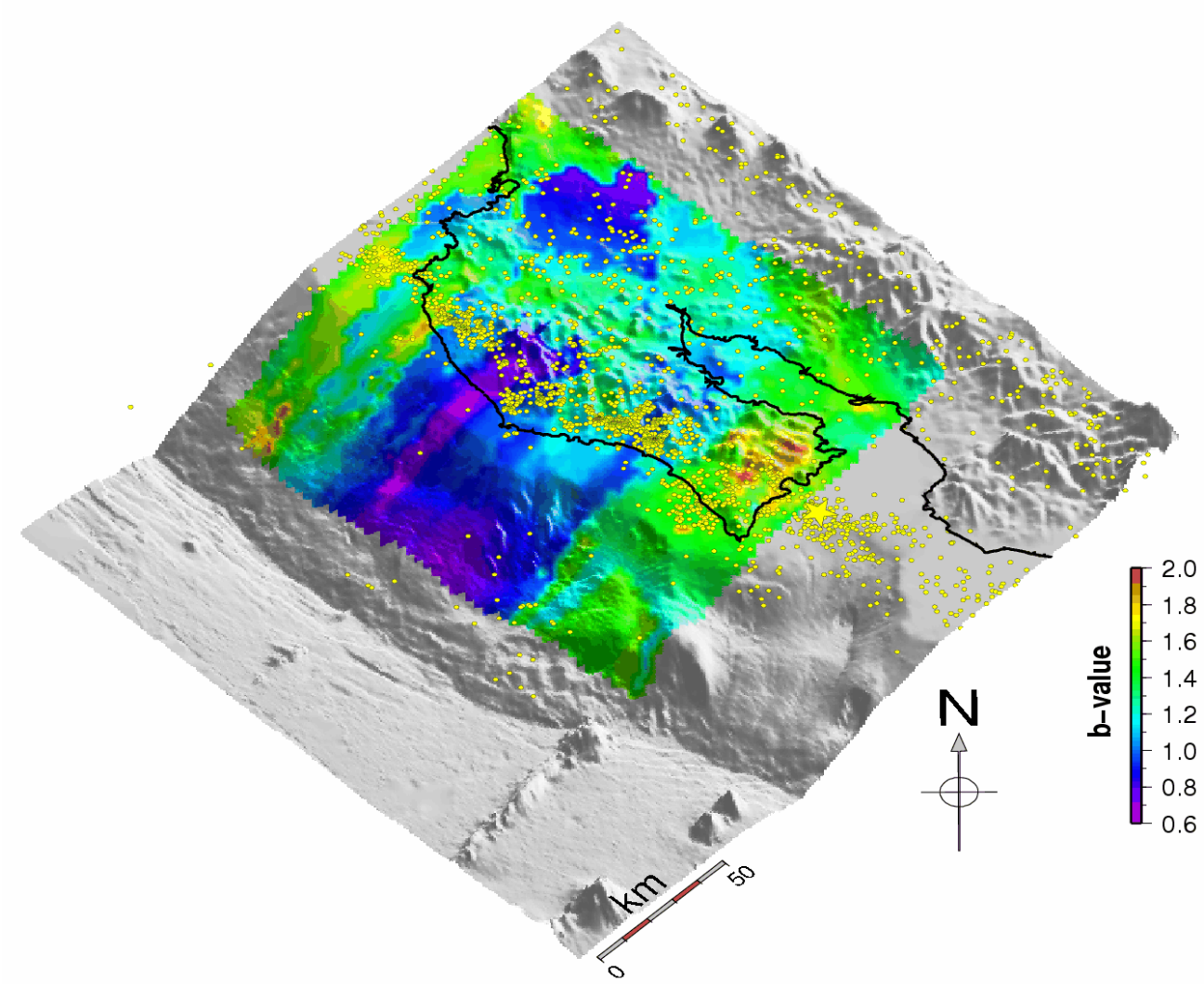

Figure 14: Spatial distribution of *b*-value calculated by the maximum likelihood method. Yellow star shows the epicenter of 1990 M_w 7.0 Gulf of Nicoya event (Protti et al., 1995b). Other features are similar to Figure 13.

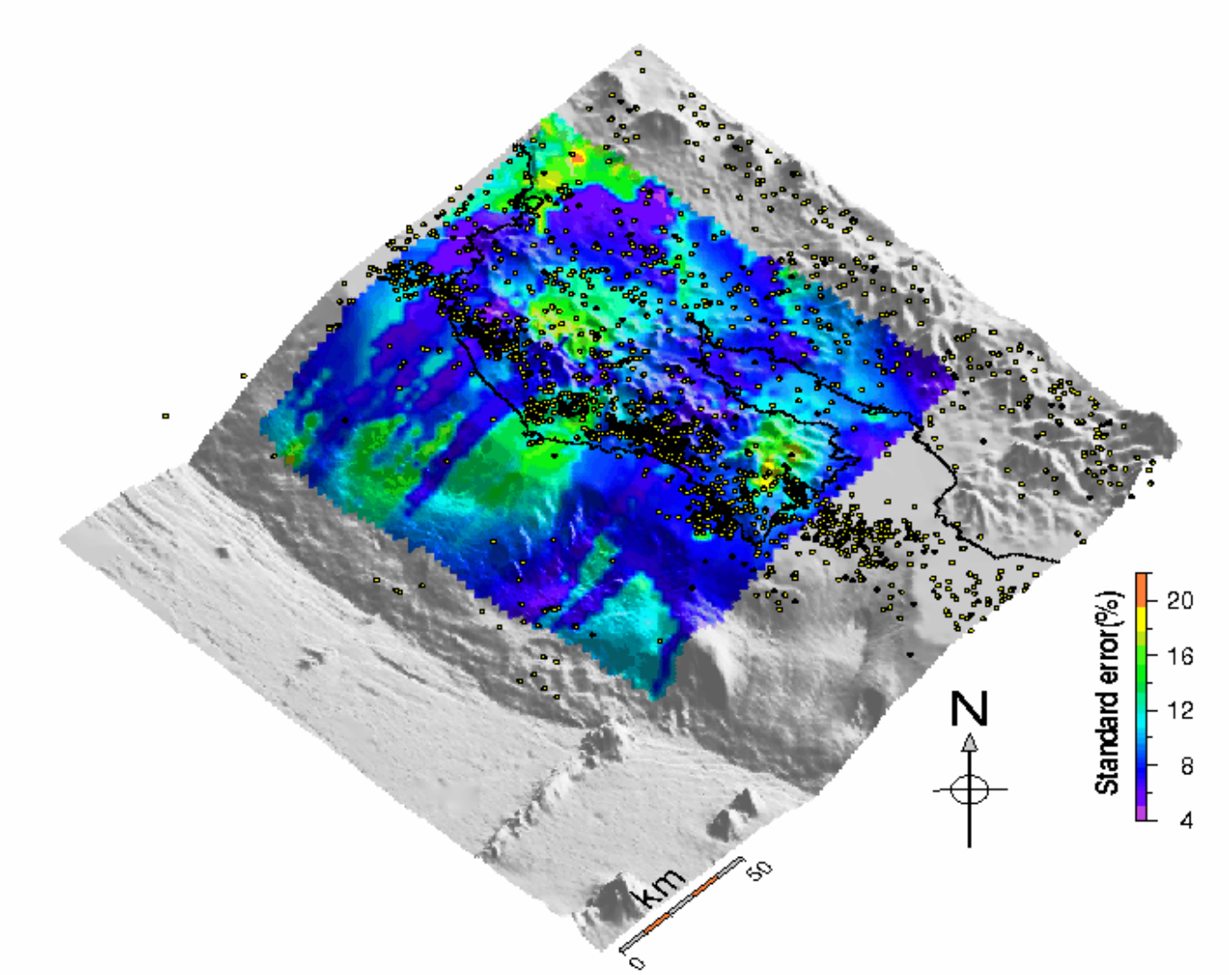

Figure 15: Spatial distribution of standard error in *b*-value estimates using the maximum likelihood method. Other features are similar to Figure 13.

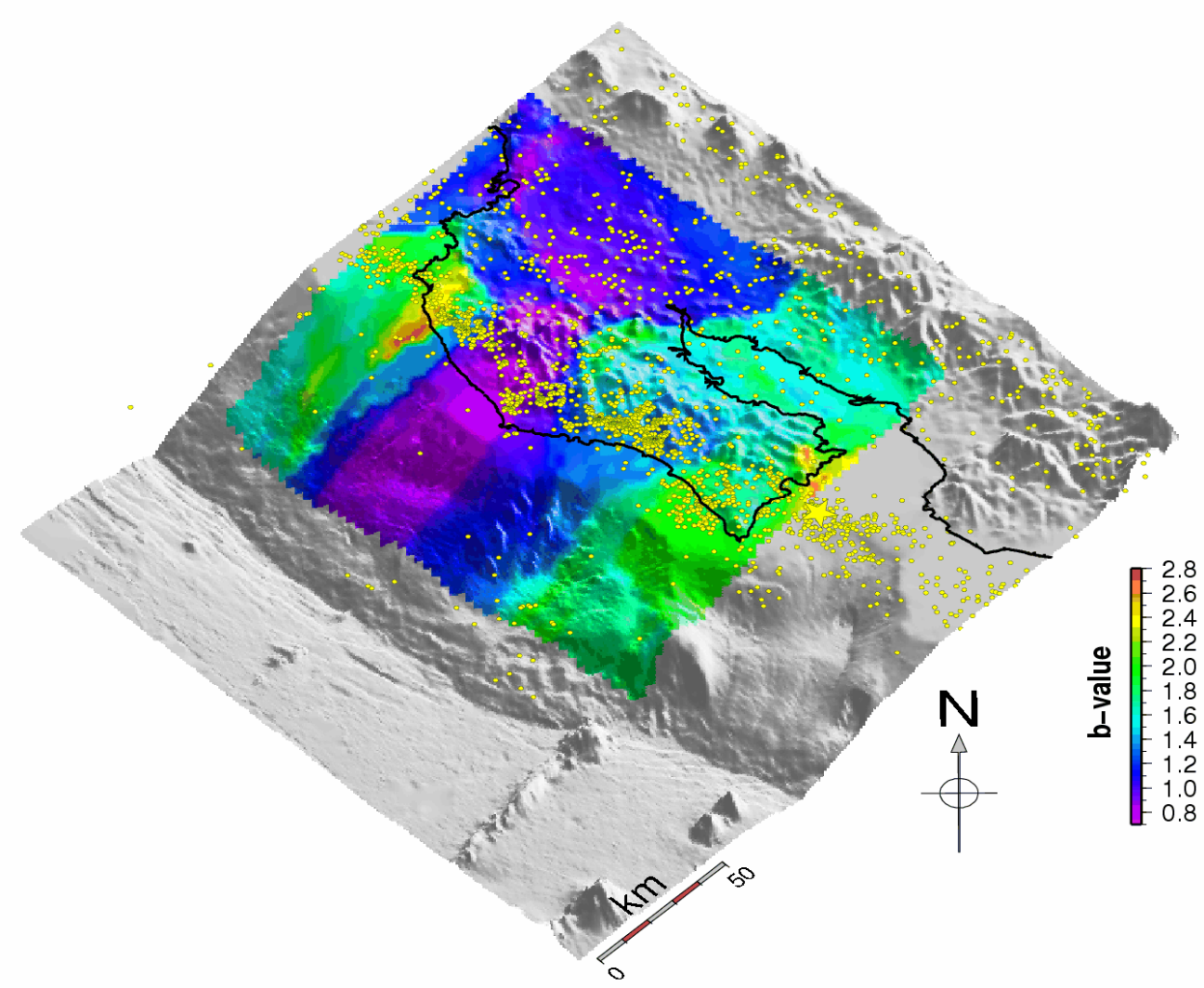

Figure 16: Spatial distribution of *b*-value calculated by the least square fit method. Yellow star shows the epicenter of 1990 M_w 7.0 Gulf of Nicoya event (Protti et al., 1995b). Other features are similar to Figure 13.

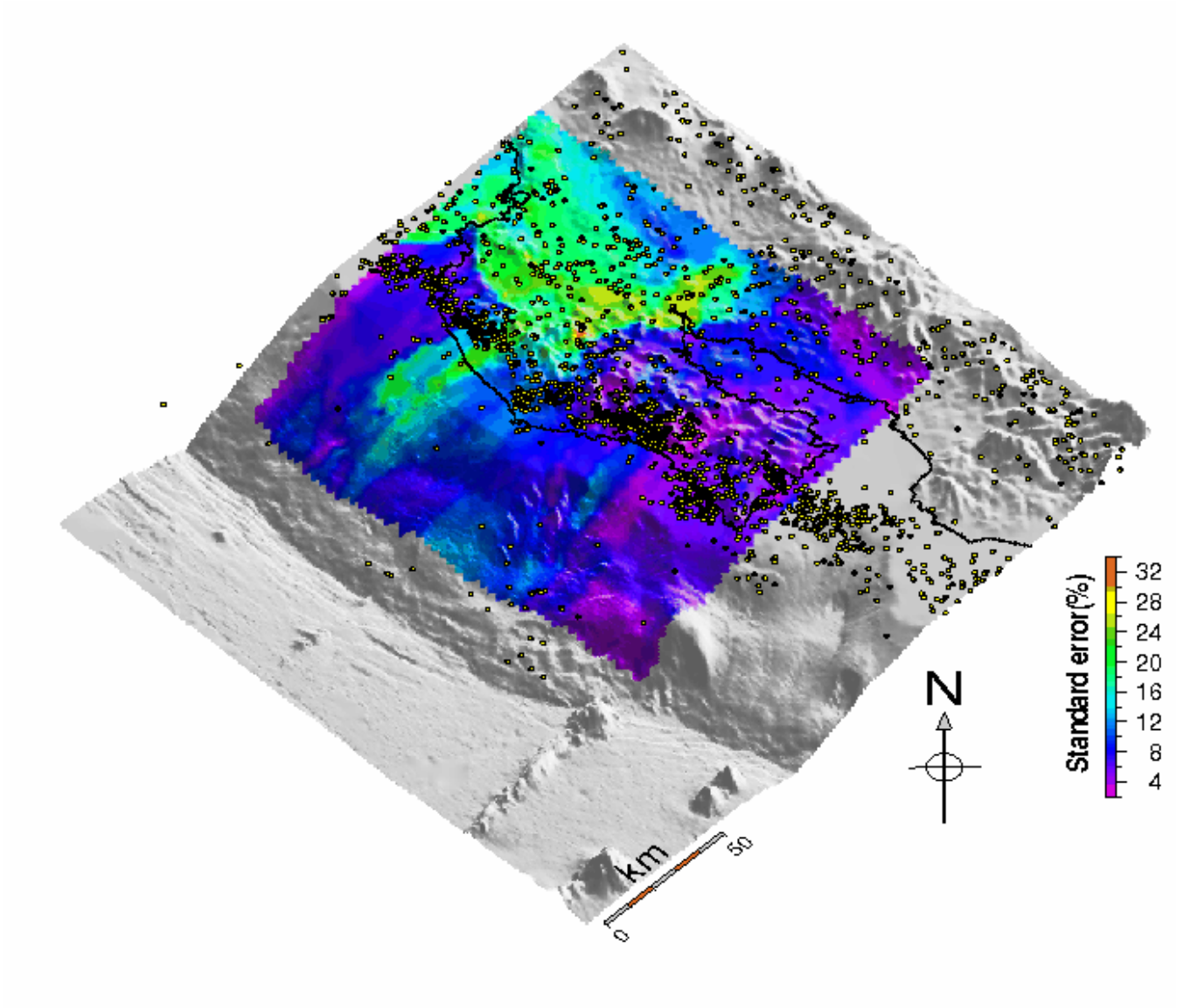

Figure 17: Spatial distribution of standard error in *b*-value estimates using the least square fit method. Other features are similar to Figure 13.

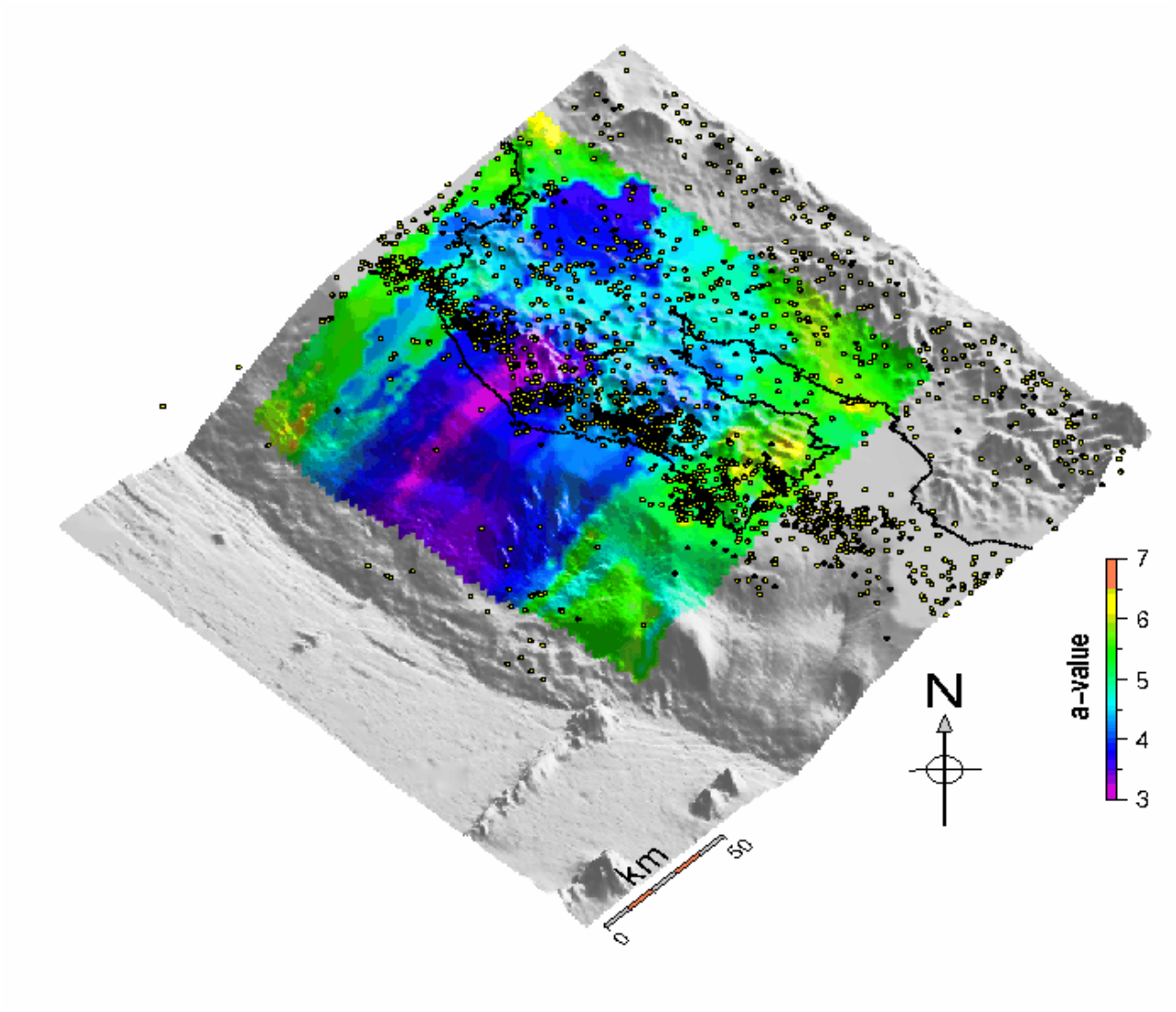

Figure 18: Spatial distribution of *a*-value calculated by the maximum likelihood method. Other features are similar to Figure 13.

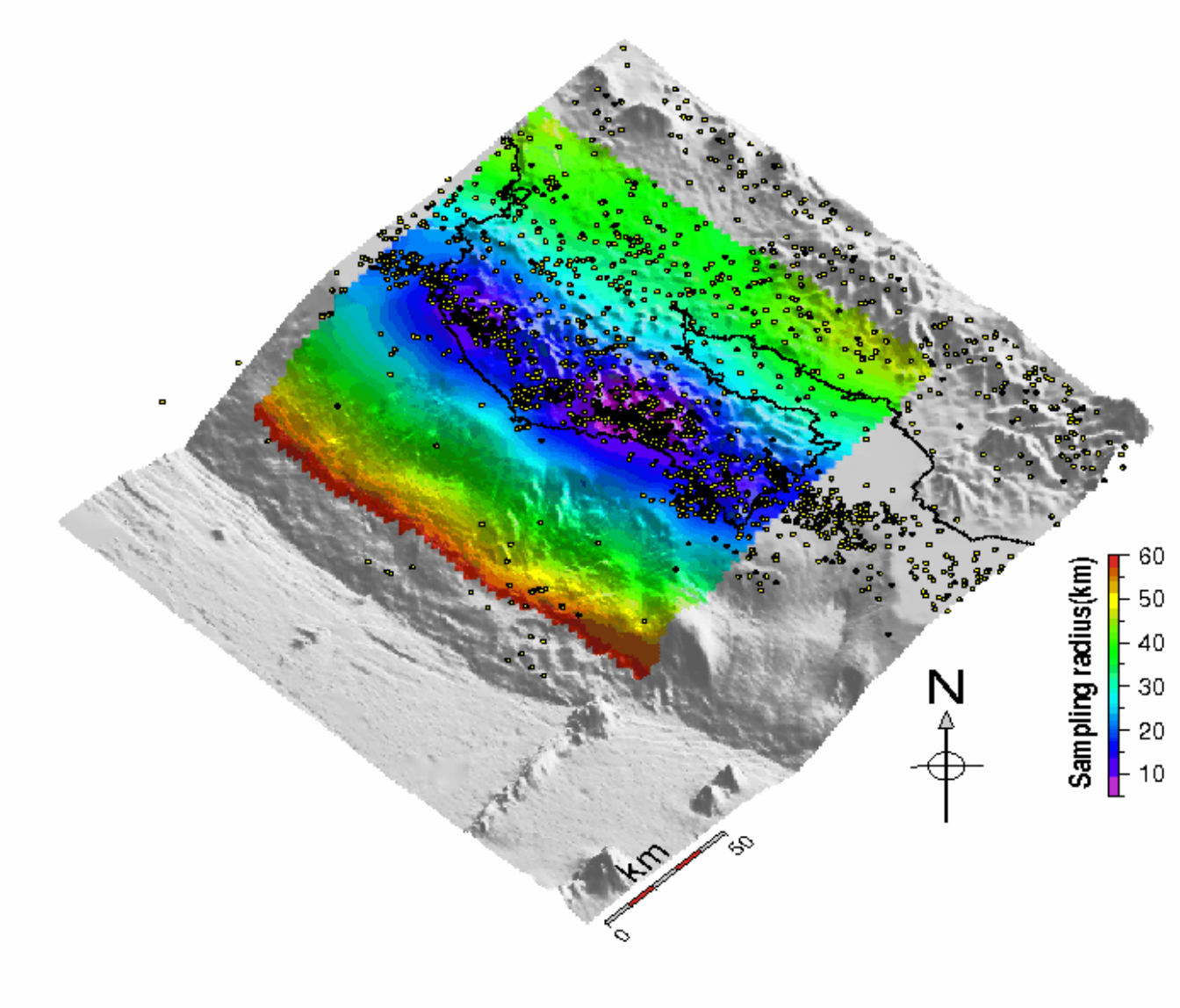

Figure 19: Spatial distribution of sampling radius in km. Other features are similar to Figure 13.

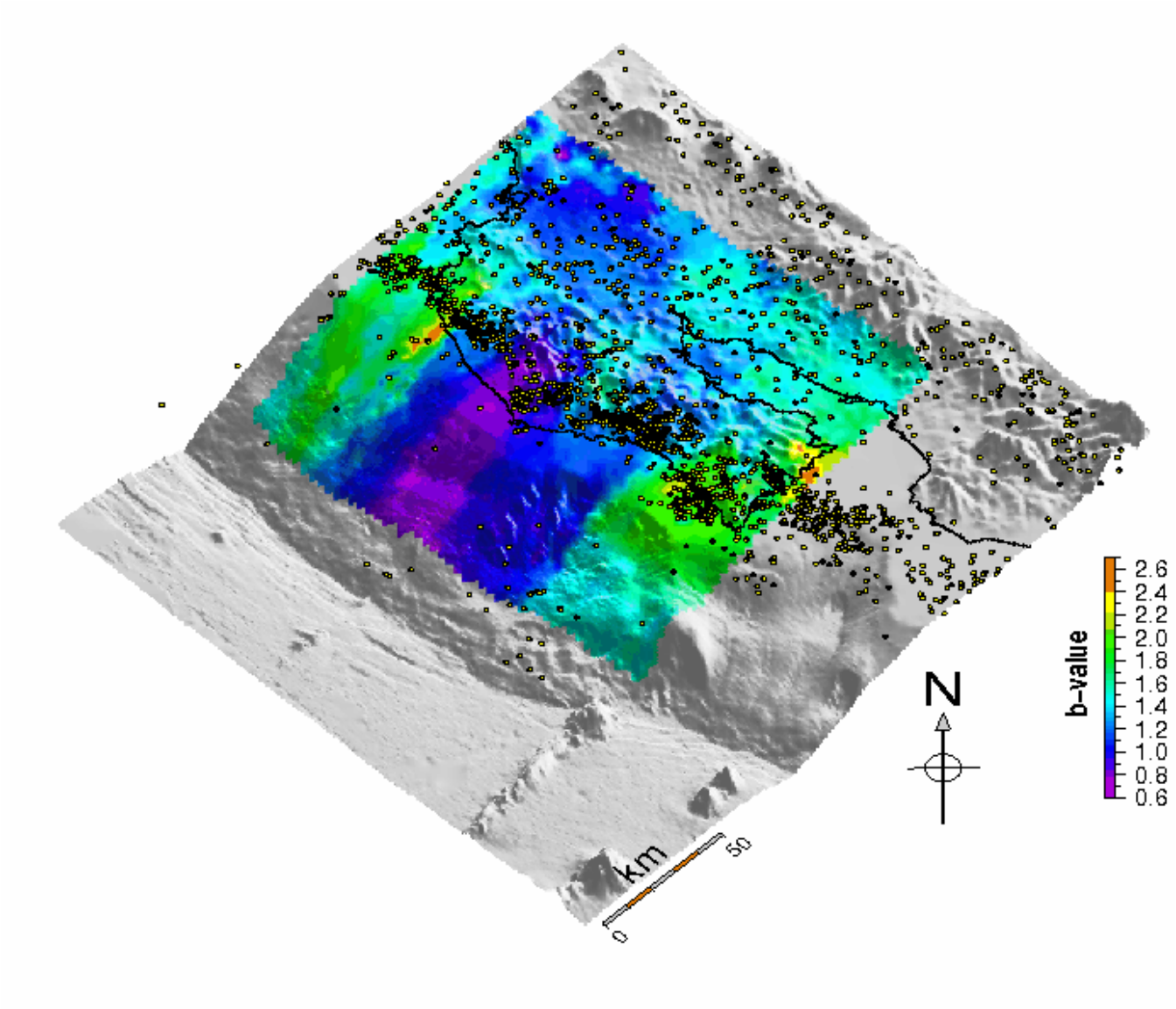

Figure 20: Spatial distribution of *b*-value calculated using the maximum likelihood method with a conservative M_C (increased by 0.2 from that calculated using maximum curvature method). Other features are similar to Figure 13.

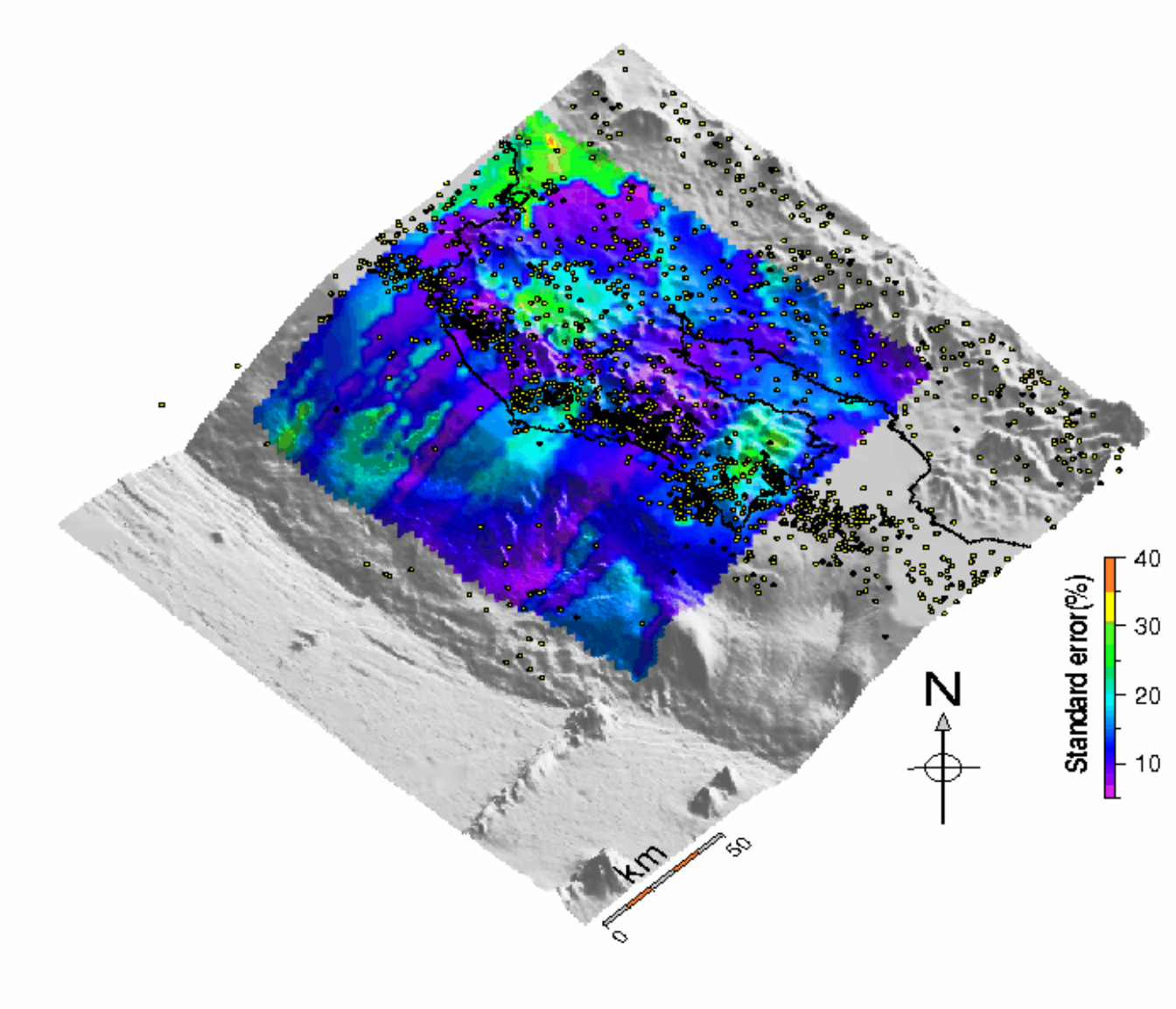

Figure 21: Spatial distribution of the standard error in the *b*-value estimated by the maximum likelihood method with a conservative M_C (increased by 0.2 from that calculated using maximum curvature method). Other features are similar to Figure 13.

The spatial distribution of *b* reveals some interesting features. Three distinct regions with anomalous *b* are found. A pronounced zone of low *b* is observed near the central Nicoya and offshore (Figure 14). This well-defined rectangular-shaped low *b* zone has value typically lower than 1. The second area with anomalously low *b*-value is observed near the northeastern corner of the Nicoya Peninsula at a greater depth of the subduction interface. It is a relatively small circular patch with *b*-value lower than 1. The third area with an anomalously high *b*-value is found to be located at the southeastern part of the peninsula. In this case, the *b*-value goes up to approximately 2. This zone of high *b* is relatively smaller in dimension than that of the low *b* regions, and approximately coincides with the landward projection of the subducting Fisher Ridge. Now the important question is: *What do these areas of anomalous b signify?*

As discussed in section 1.5, *b*-value is believed to represent the stress regime of an area, and hence, can act as a stressmeter. *b*-value is found to be inversely proportional to the differential stress in an area, such that the higher the stress, the lower the *b*-value (Schorlemmer et al., 2005). Thus, the areas of low *b* in central Nicoya and offshore, and near northeastern part of the peninsula are likely to be characterized by high stress accumulation. This state of stress may well be caused by the increased locking in part of the interface due strong seismic coupling. A strongly locked patch of the fault plane gradually accumulates stress in that part of rock volume until it slips/ruptures in a big earthquake, releasing most of the strain energy. Thus, it is reasonable to suggest that the low *b*-value zones are strongly locked and in its late stage of seismic cycle. Therefore, these regions are likely to produce the next large interface earthquake in the MASZ near Nicoya. On the other hand, the area with high *b* represents a region with relatively low stress accumulation. This area is very near the 1990 M_w 7.0, Gulf of Nicoya earthquake (Figure 14, and 16). In addition, this zone is directly above the landward projection of the Fisher Ridge and, the Gulf of Nicoya

earthquake is thought to be produced by the subducted seamount (Protti et al., 1995b). Moreover, Husen et al., (2002) showed clear tomographic image of the subducted seamount in this region. It is believed that subducted seamount can increase the seismic coupling at the seismogenic zone, and has the ability to increase the magnitude and recurrence interval of large subduction event (Scholz and Small, 1997). However, most of the stress in this part of the interface had been released by the Gulf of Nicoya event making it a zone of decreased stress concentration. Because this dataset was taken only 10 years after the event, it is in the very early stage of the seismic cycle, hence making it a good case of an area with depleted stress in that time period.

Interestingly, spatial *b*-value mapping not only reflects the stress regime on the subduction megathrust, but also corresponds well with the state of locking along the interface (Figure 22). Norabuena et al., (2004) performed an inversion of GPS data across Nicoya Peninsula from 1994 to 2000 to build a model of locking along the interface that is independent of the seismic data collected in this area. Like the *b*-value map, the GPS model also shows a strongly locked patch on the interface just offshore the central Nicoya. The locking goes up to more than 60% in this region and can possibly go up to 100% further offshore (Brown et al., 2006). The *b*-value map also delineates a profound zone of anomalously low *b* zone in this part. Likewise, another patch of low *b* at higher depth of the interface beneath northeastern part of the Nicoya Peninsula can be correlated with the second locked patch found in the GPS model at the greater depth (centered at 39 ± 6 km). Though the second low *b* zone shows weak correlation with the second geodetically derived locked patch, the pattern of distribution of low *b*-value areas and the GPS derived locked portions matches well. Norabuena et al. (2004) found two locked portions along the interface, one is at greater depth relative to other. Similarly, the spatial *b*-value map shows two zones of anomalously low *b*, at two different depths with similar spatial distribution. Moreover, the southeastern part of

the peninsula with high *b* corresponds with a zone of decreased interface locking in the GPS model (less than 20%), sitting over the down-dip extension of the Fisher Ridge. However, the shape, the spatial extent and distribution of the locked (or unlocked) patches differs slightly from zones with anomalous *b*-values, possibly because the GPS model used an assumed subduction interface that differs from the best fit interface derived on the basis of Wadati-Benioff zone seismicity in this study. The GPS model is heavily dependent on the fault plane geometry, while this FMD study has little dependence on the derived interface as events within a window of 20 km around the interface were selected.

A point-by-point comparison between *b* and locking shows a negative correlation (-0.38), meaning that *b*-value decreases as locking goes up (Figure 23). The relationship between *b* and locking is found to be, $b = 1.73 - 0.01L$, with somewhat high scatter; where *L* represent the locking in percent. These results show that variability of *b* also depicts the state of locking along this subduction interface, and the *b*-value is inversely affected by the degree of locking along the fault plane. FMD study in San Andreas Fault also revealed that the locked part of this active transform fault is marked by a zone of low *b*-value (Schorlemmer et al., 2004). While the authors of the Parkfield study mainly relied on qualitative comparison between *b* and locking, this study gives a quantitative assessment of the correlation between *b* and locking in an active fault plane. This work strongly suggests that spatial variation of *b*-value can be used to infer locking along the subduction interface based solely on the micoroseismicity.

Though inversion of GPS data showed two locked portions of along the interface, it was not able to determine whether these two patches are separated by a gradational variation of locked slip or a distinct freely slipping zone (Norabuena et al., 2004). Spatial *b*-value mapping shows that two zones of low *b* are separated by an unambiguous area of relatively higher *b* with a value close to the overall *b* for this area

(Fig. 14, and 24). It may indicate that the locked patches are separated by a freely slipping zone. Hence, in this case, FMD mapping illuminates some fine details of variability of locking that was not clearly understood by GPS modeling. Interestingly, variation in *b* also reflects the effect(s) of the interface geometry and one of the major tectonic boundaries in this region, the fracture trace separating CNS and EPR created crust. The projection of the fracture trace and the contortion at the interface at the central Nicoya corresponds with a region of typical *b* (~1.18) for this area that is situated within a broad zone that is mostly characterized by anomalously low *b* and interpreted to be the locked part on the interface (Figure 24). It appears that the low *b*-value zone in the southeastern part of the fracture trace extends farther towards land, and hence to a greater depth along the interface, than its counterpart in the northwestern side of the fracture trace. Clear variability in the distribution of *b* across the boundary between CNS and EPR crust may be caused by the variations in the physical properties (including heat flow, pore pressure, and density) and resulting stress regime between them. This observation depicts that FMD mapping not only illustrates the variation in stress and locking along the interface, but also has the ability to capture the effect(s) of major tectonic features in this area.

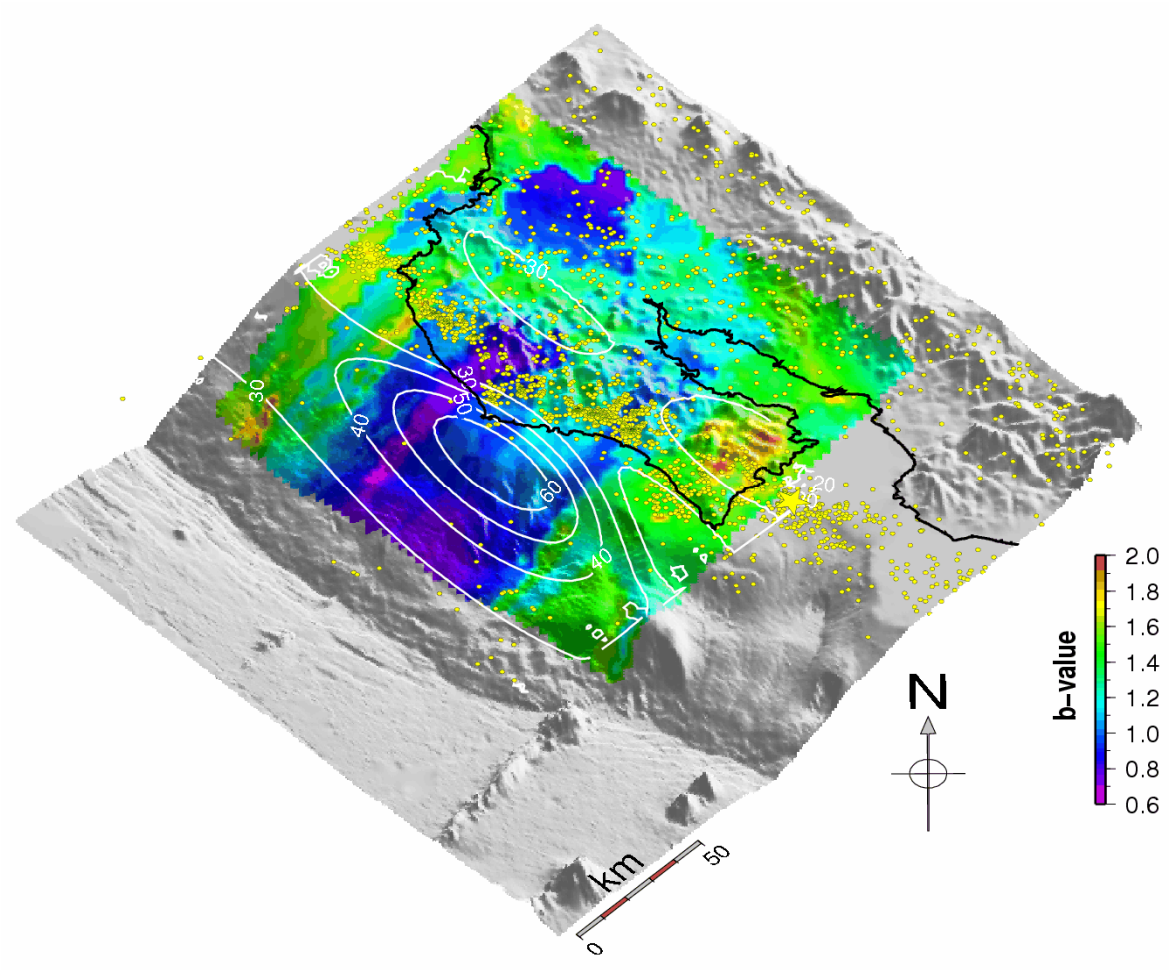

Figure 22: Spatial distribution of *b*-value calculated by the maximum likelihood method with M_C estimated by the maximum curvature method. Yellow star shows the epicenter of 1990 M_w 7.0 Gulf of Nicoya event (Protti et al., 1995b). The contour lines define the GPS derived interface locking in percent (Norabuena et al., 2004). Other features are similar to Figure 13.

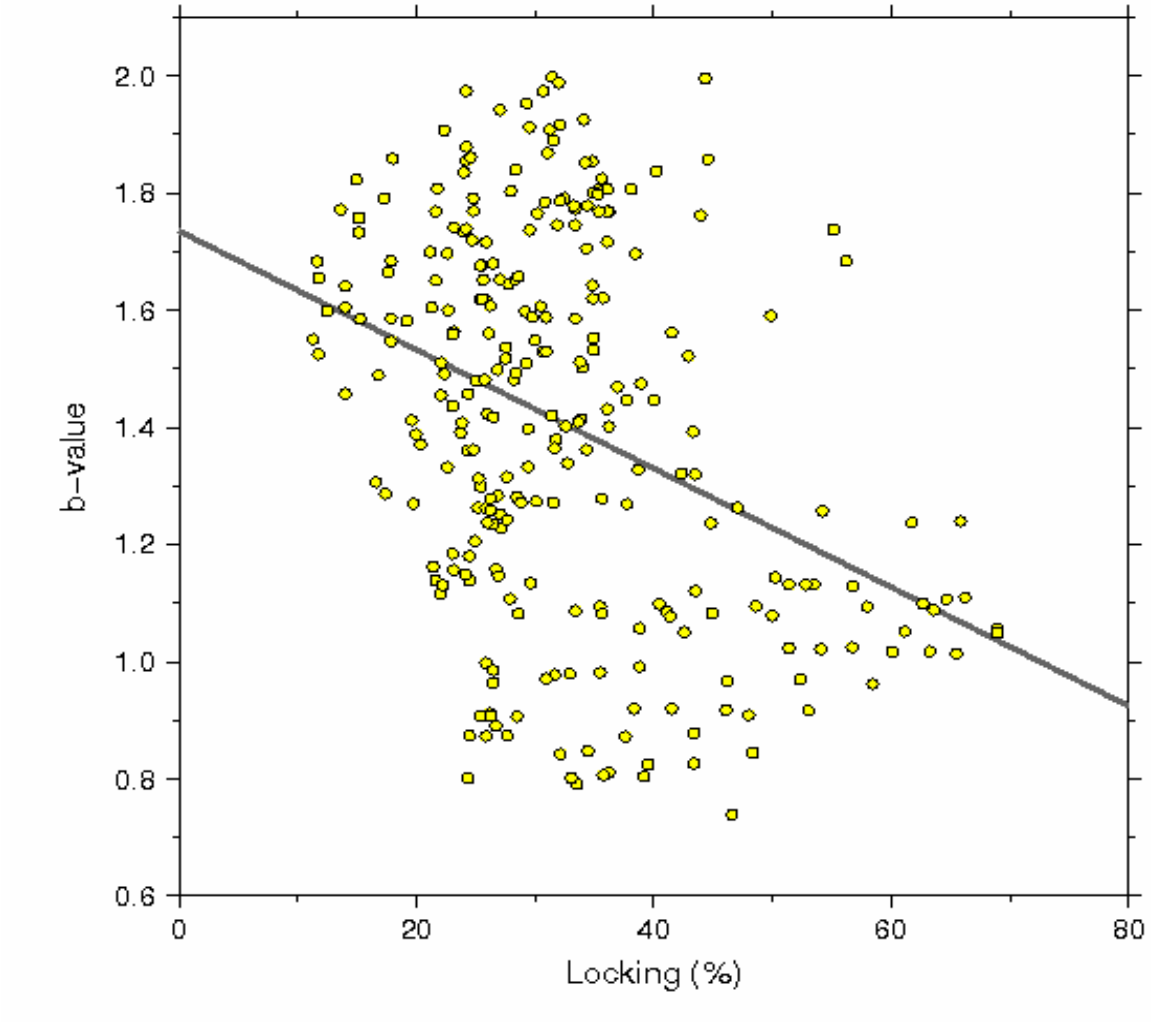

Figure 23: Direct point-by-point comparison between GPS locking (in percent) and *b*-value in maximum likelihood method. The line shows the best fit using the least square method.

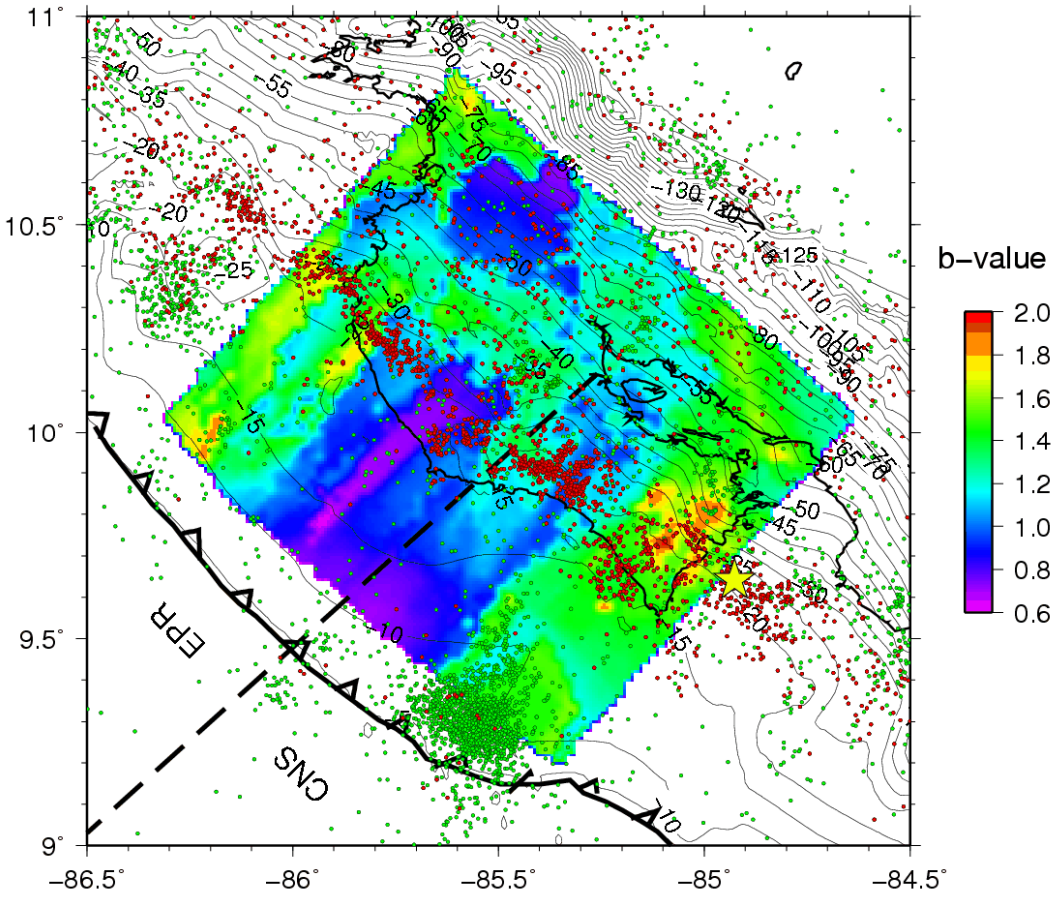

Figure 24: A summary plot of this study. Saw-toothed curve represent MAT. Green solid circles show all non-interface relocated events in the catalog. Red solid circles show only interface events with horizontal error within 5 km. Yellow star shows the epicenter of 1990 M_w 7.0 Gulf of Nicoya event (Protti et al., 1995b). Contours in km from mean sea level represent subduction interface geometry for this region derived by Thomas et al., 2007. Dashed grey line represents the trace of the fracture zone in the Cocos plate and its landward projection. The spatial distribution of *b*-value is color-coded.

CHAPTER 4

CONCLUSIONS

One of the important products of this work is a high precision regional earthquake catalog, Nicoya2000, containing 8765 relocated events in and around Nicoya Peninsula, Costa Rica. The catalog covers a time span of approximately 16 months, and reflects the seismicity along the seismogenic zone in this segment of the MASZ. The relocated aftershocks of the July 21 M_w 6.4 event suggest that the rupture and/or slip area of this large earthquake is distributed mainly on the landward part of MAT, though the mainshock is located at the outer rise of MASZ. A strong seismic lineation along the subduction interface beneath the entire Nicoya coast is observed. It is caused by rupturing of the Cocos plate due to sharp bending of the subducting slab to accommodate the abrupt large change in the dip of the interface. The subduction interface shows a contortion beneath the central Nicoya that is possibly a result of the difference in the densities between the CNS and EPR generated crust. I selected events close to the subduction interface from the Nicoya2000 catalog and analyze it in terms of it FMD. The overall b-value is found to be 1.18 ± 0.04, which suggests a moderately coupled subduction interface in this region. Spatial FMD mapping shows that there is significant variation in *b*-value along the interface. Here, *b* varies from 0.63 to 1.98 with three distinct zones of anomalous *b*. Two pronounced zones of low *b* in the central Nicoya and offshore, and beneath the northwestern part of Nicoya Peninsula at a greater depth, indicate regions with high stress accumulation and increased locking along the

interface. Conversely, a zone of high *b* in the southeastern part of Nicoya suggests low stress concentration with decreased locking. Spatial variability of *b* corresponds well with the independent GPS model of interface locking in this region (Norabuena et al., 2004). *b* is found to reflect the stress regime as well as the degree of locking on the subduction interface. Direct correlation between *b* and GPS locking suggests an inverse relationship between them, as locking increases, *b* goes down. The distribution of *b* indicates that two locked patches on the subduction interface are separated by a freely slipping part. It also shows the effect of a major tectonic boundary and the interface geometry. While inversion of geodetic data may be an optimal method for determining interface locking, assumptions about material homogeneity and precise slab geometry is necessary. Alternatively, mapping *b*-value requires fewer assumptions and can help constrain locking in regions that are not easily accessible by land-based geodetic techniques, such as updip regions of most subduction zone environments. In this work, I find that spatial *b*-value mapping of the subduction zone interface can be effectively used to infer the prevailing stress regime and the variability of degree of locking on the interface, if adequate seismic data exist.

REFERENCES

Aki, K. (1965), Maximum likelihood estimate of *b* in the formula $\log_{10} N = a - b M$ and its confidence limits, *Bull. Earthquake Res. Inst., Tokyo Univ.* 43, 237-239.

Barckhausen, U., C. R. Ranero, R. von Huene, S. C. Cande, and H. A. Roeser (2001), Revised tectonic boundaries in the Cocos plate off Costa Rica: Implications for the segmentation of the convergent margin and for plate tectonic models, *J. Geophys. Res., 106*, 19,207– 19,220.

Bayrak, Y., A. Yılmaztürk, and S. Öztürk (2002), Lateral variation of the modal (a/b) values for the different regions of the world, *J. Geodyn., 34*, 653-666.

Brown, K., A. V. Newman, R. Stevens, K. McIntosh, N. Bangs, D. Chadwell, S. Bilek, G. Spinelli, S. Schwartz, L. Dorman, E. Silver, D. Hilton, M. Kastner, G. McMurty, and G. Wheat (2006), A plate boundary observatory at Costa Rica, *MARGINS Newsletter*, Spring 2006, *16*, 19-20 (cont. 37).

Christeson, G. L., K. D. McIntosh, T. H. Shipley, E. R. Flueh, and H. Goedde (1999), Structure of the Costa Rica convergent margin, offshore Nicoya Peninsula, *J. Geophys. Res., 104(11)*, 25,443–25,468.

Darwin, C. (1845), The Voyage of the Beagle (1975 reissue), J. M. Dent, London.

DeMets, C. (2001), A new estimate for Cocos-Caribbean plate motion: Implications for slip along the Central American volcanic arc, *Geophys. Res. Lett., 28*, 4043–4046.

DeShon, H.R. (2004), Seismogenic zone structure along the Middle America subduction zone, Costa Rica, PhD thesis, University of California, Santa Cruz.

DeShon, H. R., and S. Y. Schwartz (2004), Evidence for serpentinization of the forearc mantle wedge along the Nicoya Peninsula, Costa Rica, *Geophys. Res. Lett., 31*, L21611, doi:10.1029/2004GL021179.

DeShon, H. R., S. Y. Schwartz, L. M. Dorman, A. V. Newman, V. Gonzalaz, M. Protti, T. Dixon, E. Norabuena, and E. Flueh (2006), Seismogenic Zone Structure along the Middle America Trench, Nicoya Peninsula, Costa Rica, from 3D local earthquake tomography using *P*- and *S*-wave data, *Geoph. Journ. Int., 164 (1)*, 109-124.

Evans, J. R., D. Eberhart-Phillips, and C. H. Thurber (1994), User's manual for SIMULPS12 for imaging Vp and Vp/Vs: a derivative of the Thurber tomographic

inversionSIMUL3for local earthquakes and explosions, *U.S. Geol. Surv. Open-File Report, 94–431,* U.S. Government Printing Office.

Fisher, R. L. (1961), Middle America Trench: Topography and structure, *Geol. Soc. Am. Bull., 72*, 703–720.

Fisher, A. T., C. A. Stein, R. N. Harris, K. Wang, E. A. Silver, M. Pfender, M. Hutnak, A. Cherkaoui, R. Bodzin, and H. Villinger (2003), Abrupt thermal transition reveals hydrothermal boundary and role of seamounts within the Cocos plate, *Geophys. Res. Lett., 30(11)*, 1550, doi:10.1029/2002GL016766.

Gutenberg, B., and C. F. Richter (1944), Frequency of earthquakes in California, *Bull. Seismol. Soc. Am., 34*, 185 – 188.

Hey, R. (1977), Tectonic evolution of the Cocos-Nazca spreading center, *Geol. Soc. Am. Bull., 88*, 1404–1420.

Husen, S., E. Kissling, and R. Quintero (2002), Tomographic evidence for a subducted seamount beneath the Gulf of Nicoya, Costa Rica: The cause of the 1990 M_w = 7.0 Gulf of Nicoya earthquake, *Geophys. Res. Lett., 29(8)*, 1238, doi:10.1029/2001GL014045.

Iinuma, T., M. Protti, K. Obana, V. González, R. V. der Laat, T. Kato, S. Miyazaki, Y. Kaneda, and E. Hernández (2004), Interplate coupling in the Nicoya Peninsula, Costa Rica, as deduced from a trans-peninsula GPS experiment, *Earth & Planet. Sc. Lett., 223*, 203-212.

Ishimoto, M., and K. Iida (1939), Observations of earthquakes registered with the microseismograph constructed recently, *Bull. Earthquake Res. Inst. Tokyo Univ., 17*, 443 – 478.

Lay, T., H. Kanamori, C. J. Ammon, M. Nettles, S. N. Ward, R. C. Aster, S. L. Beck, S. L. Bilek, M. R. Brudzinski, R. Butler, H. R. DeShon, G. Ekström, K. Satake, and S. Sipkin (2005), The great Sumatra-Andaman earthquake of 26 December 2004, *Science, 308(5725)*, 1127-1133, doi: 10.1126/science.1112250.

Lonsdale, P., and K. D. Klitgord (1978), Structure and tectonic history of the eastern Panama Basin, *Geol. Soc. Am. Bull., 89*, 981–999.

Lundgren, P., M. Protti, A. Donnellan, M. Heflin, E. Hernandez, and D. Jefferson (1999), Seismic cycle and plate margin deformation in Costa Rica: GPS observations from 1994 to 1997, *J. Geophys. Res., 104(B12)*, 28,915-28,926.

Mogi, K. (1962), Magnitude–frequency relations for elastic shocks accompanying fractures of various materials and some related problems in earthquakes, *Bull. Earthquake Res. Inst. Univ. Tokyo 40,* 831– 853.

Monterroso, D. A., and O. Kalhánek (2003), Spatial variation of b-values in the subduction zone of Central America, *Geofísica Internacional, 42(4)*, 575-587.

Mori, J., and R. E. Abercrombie (1997), Depth dependence of earthquake frequency-magnitude distributions in California: Implications for rupture initiation, *J. Geophys. Res., 102(B7)*, 15,081-15,090.

Newman, A. V., S. Y. Schwartz, V. Gonzalez, H. R. DeShon, J. M. Protti, and L. M. Dorman (2002), Along-strike variability in the seismogenic zone below Nicoya Peninsula, Costa Rica, *Geophys. Res. Lett., 29(20),* 1977, doi:10.1029/2002GL015409.

Nishenko, S. P. (1989), Circumpacific seismic potential 1989-1999, *U. S. Geol. Surv. Open File Rep. 89-86*.

Norabuena, E., T. H. Dixon, S. Y. Schwartz, H. R. DeShon, A. V. Newman, M. Protti, V. Gonzalez, L. M. Dorman, E. Flueh, P. Lundgren, F. Pollitz, and D. Sampson (2004), Geodetic and seismic constraints on some seismogenic zone processes in Costa Rica, *J. Geophys. Res., 109*, B11403, doi:10.1029/2003JB002931.

Nuannin, P., O. Kulhanek, and L. Persson (2005), Spatial and temporal b value anomalies preceding the devastating off coast of NW Sumatra earthquake of December 26, 2004, *Geophys. Res. Lett., 32*, L11307, doi:10.1029/2005GL022679.

Okada, Y. (1985), Surface deformation due to shear and tensile faults in a half-space, *Bull. Seismol. Soc. Am. 75*,1135–1154.

Protti, M., F. Guendel, and K. McNally (1995a), Correlation between the age of the subducting Cocos plate and the geometry of the Wadati-Benioff zone under Nicaragua and Costa Rica, in *Geologic and Tectonic Development of the Caribbean Plate Boundary in Southern Central America*, edited by P. Mann, Spec. Pap. Geol. Soc. Am., 295, 309–326.

Protti, M., K. McNally, J. Pacheco, V. Gonzales, C. Montero, J. Segura, J. Brenes, V. Barboza, E. Malavassi, F. Güendel, G. Simila, D. Rojas, A. Velasco, A. Mata, and W. Schillinger (1995b), The March 25, 1990 (Mw = 7.0, M_L = 6.8) earthquake at the entrace of the Nicoya Gulf, Costa Rica: Its prior activity, foreshocks, aftershocks, and triggered seismicity, *J. Geophys. Res., 100(B10)*, 20,345–20,358.

Reyners, M. (1998), Plate coupling and the hazard of large subduction thrust earthquakes at the Hikurangi subduction zone, New Zealand, *The Roy. Soc. New Zealand, 41*, 343-354.

Sallarès, V., J. J. Dañobeitia, E. R. Flueh, and G. Leandro (1999), Seismic velocity structure across the Middle American landbridge in northern Costa Rica, *J. Geodyn., 27*, 327– 344.

Sallarès, V., J. J. Dañobeitia, and E. R. Flueh (2001), Lithospheric structure of the Costa Rica Isthmus: Effects of subduction zone magmatism on an oceanic plateau, J*. Geophys. Res., 106*, 621– 643.

Scheaffer, R. L., and J. T. McClave (1986), *Probability and Statistics for Engineeres*, Duxbury Press, Boston.

Scholz, C. H. (1968), The frequency–magnitude relation of microfracturing in rock and its relation to earthquakes, *Bull. Seismol. Soc. Am. 58*, 399–415.

Scholz, C. H., and C. Small (1997), The effect of seamount subduction on seismic coupling, *Geology, 25*, 487– 490.

Schorlemmer, D., and S. Wiemer (2005), Microseismicity data forecast rupture area, *Nature 434*, 1086.

Schorlemmer, D., G. Neri, S. Wiemer, and A. Mostaccio (2003), Stability and significance tests for *b*-value anomalies: Example from the Tyrrhenian Sea, *J. Geophys. Res. 30(16)*, 1835, doi:10.1029/2003GL017335.

Schorlemmer, D., S. Wiemer, and M. Wyss (2004), Earthquake statistics at Parkfield: 1. Stationarity of b-values. *J. Geophys. Res. 109*, B12307, doi:10.1029/2004JB003234.

Schorlemmer, D., S. Wiemer and M. Wyss (2005), Variation in earthquake-size distribution across different stress regimes, *Nature, 437(22)*, 539-542, doi:10.1038/nature04094.

Shi, Y., and B. A. Bolt (1982), The standard error of the magnitude-frequency *b* value, *Bull. Seismol. Soc. Am., 72 (5),* 1677-1687.

Stein, S. & M. Wysession (2003), *An Introduction to Seismology, Earthquakes, and Earth Structure*, Oxford: Blackwell Publishing.

Thomas, A. M., A. V. Newman, A. Ghosh, and G. T. Farmer (2007), Statistical modeling of the Middle America Subduction Zone using interplate seismicity, paper presented at 2007 Seismological Society of America Annual Meeting, Big Island, Hawaii, 11-13 April.

Thurber, C. H. (1983), Earthquake locations and and three-dimensional crustal structure in the Coyote Lake area, central California, *J. Geophys. Res. 88(B10)*, 8226-8236.

Warren, N. W., and G. V. Latham (1970), An experiment study of thermal induced microfracturing and its relation to volcanic seismicity, *J. Geophys. Res., 75*, 4455–4464.

Wesnousky, S. G. (1994), The Gutenberg-Richter or characteristic earthquake distribution, which is it?, *Bull. Seismol. Soc. Am., 84(6),* 1940-1959.

Wiemer, S. (2001), A software package to analyze seismicity: ZMAP, *Seismol. Res. Lett., 72*, 373 – 382.

Wiemer, S., and J. P. Benoit (1996), Mapping the b-value anomaly at 100 km depth in the Alaska and New Zealand subduction zones, *Geophys. Res. Lett., 23(13)*, 1557-1560.

Wiemer, S., and S. R. McNutt (1997), Variation in the frequency-magnitude distribution with depth in two volcanic areas: Mount St. Helens, Washington, and Mt. Spurr, Alaska, *Geophys. Res. Lett., 24(2)*, 189-192.

Wiemer, S., and M. Wyss (1997), Mapping the frequency– magnitude distribution in asperities: An improved technique to calculate recurrence times? *J. Geophys. Res. 102*, 15115– 15128.

Wiemer, S., and K. Katsumata (1999), Spatial variability of seismicity parameters in aftershock zones, *J. Geophys. Res., 103*, 13,135–13,151.

Wiemer, S., and M. Wyss (2000), Minimum magnitude of completeness in earthquake catalogues: Examples from Alaska, the western United States, and Japan, *Bull. Seismol. Soc. Am., 90,* 859-869.

Wilson, D. S., and R. Hey (1995), History of rift propagation and magnetization intensity for the Cocos-Nazca spreading center, *J. Geophys. Res., 100*, 10,041–10,056.

Wyss, M. (1973), Towards a physical understanding of the earthquake frequency distribution, *Geophys. J. R. Astron. Soc., 31*, 341 – 359.